

Diverse patterns of ascent, degassing, and eruption of rhyolite magma during the 1.8 ka Taupo eruption, New Zealand: Evidence from clast vesicularity

Bruce F. Houghton^{a,*}, Rebecca J. Carey^a, Katharine V. Cashman^b, Colin J.N. Wilson^c,
Barbara J. Hobden^d, Julia E. Hammer^a

^a Department of Geology and Geophysics, University of Hawai'i, 1680 East-West Road, Honolulu, HI 96822, USA

^b Department of Geological Sciences, University of Oregon, Eugene, Oregon 97403, USA

^c School of Geography, Environment and Earth Sciences, Victoria University, Wellington 6140, New Zealand

^d Department of Earth Sciences, University of Waikato, Hamilton, New Zealand

ARTICLE INFO

Article history:

Received 12 February 2010

Accepted 9 June 2010

Available online 21 June 2010

Keywords:

explosive volcanism

vesiculation

conduit process

Plinian

Taupo eruption

ABSTRACT

The 22 km³ (DRE) 1.8 ka Taupo eruption ejected chemically uniform rhyolite in a wide range of eruptive styles and intensities. The 7 eruptive units include the 'type examples' of phreatoplinian (units 3 and 4) and ultraplinian fall (unit 5) deposits, and low-aspect-ratio ignimbrite (unit 6). Contrasts in bulk vesicularity, vesicle (and microlite) number densities and the size distributions of bubbles (and crystals) in the Taupo ejecta can be linked to the influence of shallow conduit processes on volatile exsolution and gas escape, before and during eruption, rather than changes in pre-eruptive chemistry. Existing work has modeled the individual phases of this complex eruption but not fully explained the abrupt shifts in style/intensity that occur between phases. We link these rapid transitions to changes in vent position, which permitted contrasts in storage, conduit geometry, and magma ascent history.

Samples in the study show that coalescence of bubbles was a late-stage process in the pre-fragmentation degassing of even the most rapidly ascending magma, but, in most cases, nucleation of new bubbles continued until close to fragmentation. In the two phases of the Taupo eruption linked to dome or cyptodome formation, we can also recognize an influence of onset of permeability, partial outgassing, limited syn-eruptive crystallization, and bubble collapse. Post-fragmentation expansion or contraction of vesicles was only marked in some pumices within the deposits of the two heat-retentive yet nonwelded pyroclastic density currents (units 5B and 6).

We can recognize three different types of history of ascent, bubble nucleation, and degassing for the Taupo eruption. Units 1, 2, 3, 5, and 6 involved magma that ascended rapidly under the southern and central portions of the vent system and underwent late-stage closed system, coupled vesiculation without syn-eruptive crystallization of microlites. The limited contrasts in textures amongst these units reflect only slightly different ascent histories, including slower rise permitting extended bubble coalescence (unit 1), rapid, accelerating ascent (units 2, 3 and 5), and exceptionally rapid decompression and ascent at the time of highest mass discharge rates (unit 6).

In contrast to all these units, the unit 4 magma also rose rapidly initially but then underwent some degree of limited and shallow storage, permitting variable degrees of prolonged bubble maturation (growth and coalescence), development of permeability and outgassing, under the northern portion of the 10-km-long vent system, probably beginning at the time of eruption of units 1–3 from the southern portion of the fissure. Finally, the magma which formed the late-stage dome (unit 7), remained deeper in the plumbing system for an extended time permitting limited growth of microphenocrysts, (perhaps in response to partial depressurisation occurring during the earlier phases of the eruption), before ascending and continuing to outgas in equilibrium fashion.

© 2010 Elsevier B.V. All rights reserved.

1. Introduction

1.1. Explosive eruption mechanisms and controls

The mechanisms and dynamics of large explosive eruptions represent formidable challenges to understanding whether for past eruptions, ongoing activity, or for future eruptive events. Such eruptions

* Corresponding author. Tel.: +1 808 9562561; fax: +1 808 9565512.

E-mail address: bhought@soest.hawaii.edu (B.F. Houghton).

may be highly destructive, often showing complex and seemingly random behavior in parameters such as eruptive intensity, which may vary by over 7 orders of magnitude (Table 1). Stable buoyant (Plinian) plumes may give way gradually or abruptly to dome growth, or paroxysmal pyroclastic density currents, or phreatomagmatic explosions, or an abrupt cessation of activity. Volcanologists are as yet unable to explain many aspects of this divergence in style and intensity, or, more importantly, to predict the behaviour of future large eruptions.

Reducing the human cost of volcanic crises requires better knowledge of what factors control the style and intensity of large explosive eruptions. The scale of all explosive eruptions of a size capable of being represented in the geological record inhibit close direct observations, and much of our understanding of such events derives from studies of the resulting pyroclastic products, coupled with geophysical data in active eruptions, and analogue and numerical modeling. From these data and models, there is now widespread acceptance of a number of basic controls on explosive eruption behavior.

In general, eruption intensity, duration and style are considered to be determined within either the region of magma storage, which provides the overpressure driving an eruption, or the volcanic conduit, where magma decompresses, loses volatiles, and sometimes partially crystallizes (Wilson et al., 1980; Jaupart and Tait, 1990; Jaupart and Allegre, 1991; Woods and Koyaguchi, 1994; Jaupart, 1996; Bower and Woods, 1998; Massol and Jaupart, 1999; Huppert, 2000; Papale, 2001; Gonnermann and Manga, 2007; Scandone et al., 2007). Even for the simplest of cases, with a magma with uniform chemical composition and initial volatile content, complex changes in eruptive style or intensity may be driven by:

- (a) changing flow behaviour in the conduit (e.g., Kaminski and Jaupart, 1997; Papale et al., 1998; Denlinger and Hoblitt, 1999) as magma rheology alters in response to the changes in the concentrations of dissolved volatiles, bubbles and crystals (e.g., Hess and Dingwell, 1996; Manga et al., 1998; Papale et al., 1998; Llewellyn and Manga, 2005; Massol and Koyaguchi, 2005; Gonnermann and Manga, 2007), or
- (b) external environmental factors, such as widening of the conduit or the influx of external water (e.g., Barberi et al., 1989; Koyaguchi and Woods, 1996; Carey et al., 2009).

One key insight into conduit processes is the imprint that they leave on the microtextures of the eruption products (Cashman, 1992; Cashman and Mangan, 1994; Klug and Cashman, 1994; Gardner et al., 1996; Hammer et al., 1998, 1999; Mourtada-Bonnefoi and Mader, 2004; Carey et al., 2009). In many cases complexities in the characteristics of single pyroclasts or deposits can be shown to have arisen because of four additional factors:

- (i) The presence of some form of compositional zonation in the magma chamber, which leads to systematic variations in the

magma properties (e.g., viscosity and initial volatile content). These changing properties may act in addition to the physical controls listed above in controlling the style of eruptions. Notable examples of such compositional variations are the AD 79 eruption of Vesuvius (e.g., Cioni, 2000; Gurioli et al., 2005; Shea et al., 2009), and the 1912 eruption of Novarupta (Fierstein and Hildreth, 1992; Hildreth and Fierstein, 2000; Houghton et al., 2003; Adams et al., 2006a).

- (ii) The presence of single versus multiple vents. If the magma is emplaced as a dike in the upper crust, multiple vents may erupt simultaneously or sequentially along the dike, with each vent (in principle) having the opportunity to show different behavior controlled by local parameters such as those listed in (a) and (b), above. Notable examples of this have occurred in basaltic fissure eruptions, such as Laki 1783 (Thordarson and Self, 1993) and Tarawera, 1886 (e.g., Sable et al., 2006, 2009; Carey et al., 2007) and are also known from rhyolite eruptions like Kaharoa 1314 (e.g., Nairn et al., 2001).
- (iii) The possibility of eruptive breaks, which may occur in single- or multiple-vent eruptions (e.g., Nairn et al., 2001; Adams et al., 2006a) and are a challenge to quantify in any prehistoric eruption. Estimating the duration of such breaks is, however, important in disentangling the effects on magma properties of processes like gas loss and microlite growth, and deciphering whether these might have occurred prior to a continuous, uninterrupted eruption (e.g., in a shallow intrusion) or during time breaks in an episodic eruption. In addition, the recognition of eruptions starting and stopping may give valuable insights into the controls and feedback loops involved in magma chamber behaviour and how and when conduits are open or closed.
- (iv) The presence of complex relationships between buoyant and non-buoyant plumes, the latter leading to the generation of pyroclastic density currents (PDCs). This contrast may be expressed as a one-way change from fall to pdc, or oscillatory behavior between the two regimes, or may reflect simultaneous contrasts in behavior of a single eruption plume. The buoyant/non-buoyant transition may be coincident with (i) that influences or merely accompanies the changing eruption style (e.g., Fierstein and Hildreth, 1992; Houghton et al., 2004; Gurioli et al., 2005).

To illustrate the ways in which these complexities may be disentangled through a combination of field-based and clast-specific observations, we address conduit and vent processes in the 1.8 ka eruption of Taupo volcano, New Zealand (Walker, 1980, 1981a,b; Walker and Wilson, 1985; Wilson, 1985; Smith and Houghton, 1995). This complex eruption of c. 35 km³ magma demonstrates three of the four complexities outlined above, having evidence for multiple vents,

Table 1
Characteristics of the Taupo eruption, in comparison with documented 20th century silicic eruptions.

Eruption	Max inferred plume (km)	Vol DRE (km ³)	SiO ₂ mtx glass (wt.%)	Phenocrysts (wt.%)	Range of mass discharge rate (kg s ⁻¹)	
					min	max
181 AD Taupo ¹	55	35	74	2–3.5	10 ³	10 ¹⁰
1991 Pinatubo ²	40	4–5	68–77	15–47	10 ³	10 ⁹
1912 Novarupta ³	26	13	73–78	2–50	10 ³	10 ⁸
1875 Askja ⁴	28	0.3	69–73	<1	10 ⁶	10 ⁸
1980–6 St Helens ⁴	25	1	68–80	30	10 ³	10 ⁷
1995 – Soufriere Hills ⁶	15	.08	76–79	45–55	10 ²	10 ⁶
1991–5 Unzen ⁷	<14	0.2	74–79	23–28	10 ²	10 ⁴

References: 1: Sutton et al. (1995, 2000), Wilson and Walker (1985), Wilson (1993); 2: Koyaguchi and Woods (1996); 3: Fierstein and Hildreth (1992), Hammer et al. (1999), Houghton et al. (2004); 4: Sparks (1978), Carey et al. (2009); 5: Blundy and Cashman (2001, 2005); 6: Melnik and Sparks (1999, 2002); 7: Nakada et al. (1999), Nakada and Motumura (1999).

Table 2

Summary of the deposits and eruptive styles during the 1.8 ka Taupo eruption, modified after Wilson and Walker (1985).

Unit	Stratigraphic name	Type of deposit	Style	Rate (kg s ⁻¹)
7	Floating blocks	dome	Fubaqueous dome growth	? 10 ³
6	Taupo ignimbrite	pdcc	Widespread density current	10 ¹⁰
5	Taupo Plinian/early ignimbrite	fall/pdcc	Powerful Plinian + pdcc and localised flow activity	10 ⁸
4	Rotongaio phreatoplinian	fall	Phreatoplinian, dense juvenile clasts	10 ⁶
3	Hatepe phreatoplinian	fall	Phreatoplinian, pumiceous clasts	10 ⁶
2	Hatepe Plinian	fall	Moderate Plinian	10 ⁷
1	Initial ash	fall	Weak phreatomagmism	10 ⁵

time breaks between events, and simultaneous and sequential production of fall and PDC deposits (Table 2). The eruption is equally remarkable for the lack of compositional zonation with respect to either volatiles or major and trace elements (Dunbar and Kyle, 1993; Sutton et al., 1995, 2000; see below) which means that a uniform starting state for the magma can be assumed in interpreting

degassing, vesiculation and fragmentation histories for pyroclasts. The Taupo eruption is thus a valuable case study to approach the dynamics of large explosive volcanic eruptions because of the wide range of eruptive styles and intensities, together with the comparisons that can be made between the macroscopic characteristics of the deposits and clast-specific microtextural information.

1.2. The 1.8 ka Taupo eruption

The eruption at 1.8 ka is the youngest event at Taupo volcano in the central Taupo Volcanic Zone of New Zealand (Fig. 1). The volcano is unusual on a world scale in having experienced two young rhyolitic caldera-forming eruptions at 27 and 1.8 ka. Between these events, 26 other explosive and dome-building eruptions have occurred, making Taupo the world's most frequently active rhyolite volcano (Wilson, 1993). The Taupo eruption, as interpreted by Wilson and Walker (1985), and here, consisted of two unequal parts: an earlier complex sequence of explosive phases ("eruption Y" of Wilson, 1993) and a later effusive phase ("eruption Z" op. cit.) following a time break of some years to decades. The eruption was the second largest known globally in the last

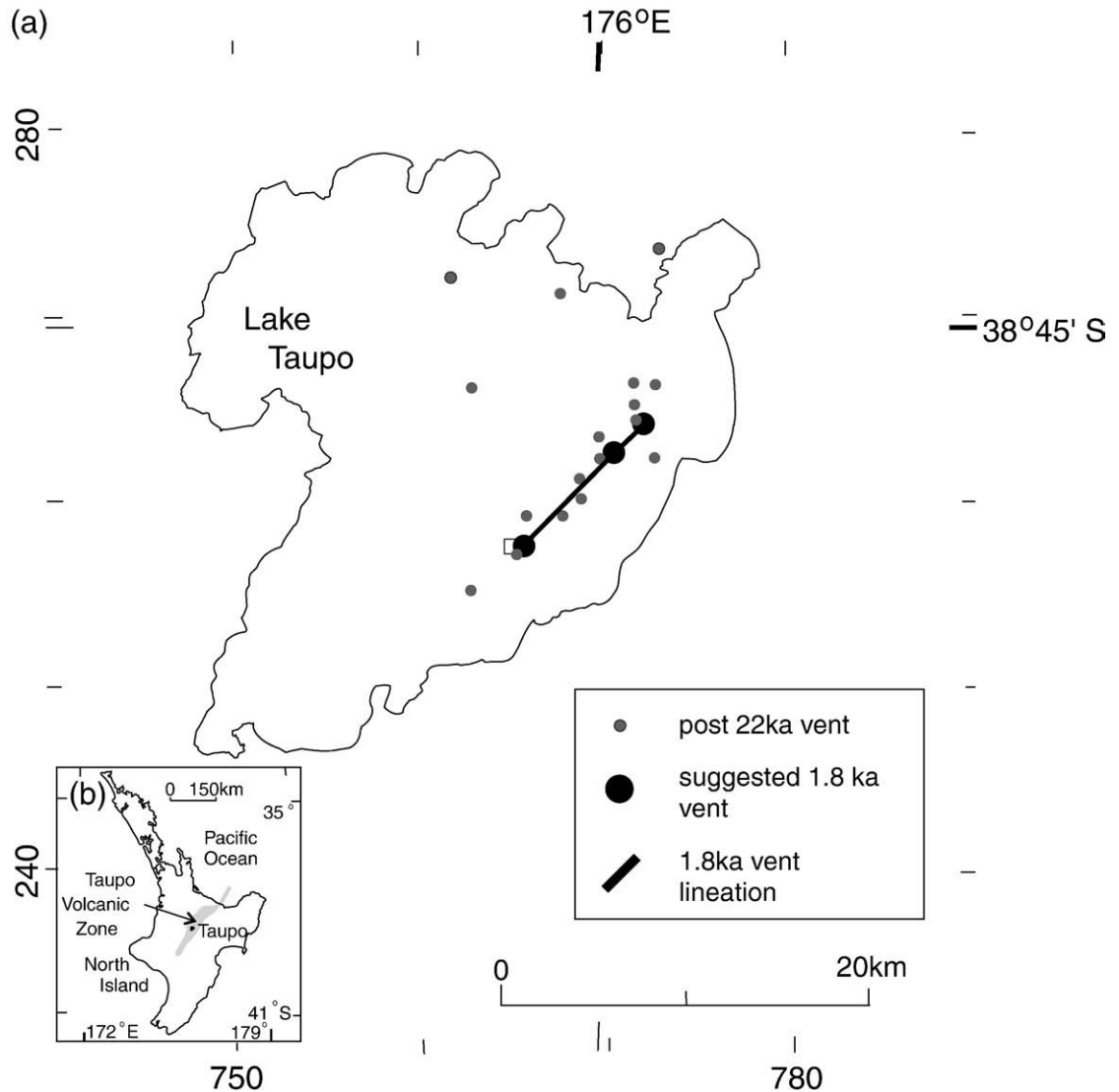


Fig. 1. (a) Taupo volcano showing the location of all vents active in the last 22,000 years (after Wilson 1993). Postulated vents for the 1.8 ka eruption are shown by larger black dots, after Wilson and Walker (1981) and Smith and Houghton (1995). (b) Location map for Taupo volcano within the Taupo Volcanic Zone, New Zealand. Map co-ordinates in Latitude/longitude in addition to UTM.

2000 years, and probably the most powerful world-wide in the last 5000 years. The eruption is notable for several reasons:

- Its great diversity of eruptive styles (Table 2), generating two dry Plinian fall deposits, three phreatomagmatic fall deposits, multiple intraplinian ignimbrite flow units, and a climactic widespread flow deposit that is the archetype for low-aspect ratio ignimbrites (Walker, 1980, Walker 1981a,b; Wilson, 1985).
- The extreme vigor of the second Plinian phase and the climactic pdc; the latter has the highest inferred mass discharge rate ($\sim 7 \times 10^{10} \text{ kg s}^{-1}$; Wilson & Walker, 1980) for any young eruption.
- Its multiple-vent nature. Although originally interpreted to be erupted from a single vent (Walker, 1980), detailed studies of the units 3 and 4 by Smith and Houghton (1995) have indicated the presence of other sources to the SSW (unit 3, and also unit 1, as reinterpreted by Houghton et al., 2003) and NNE of Walker's vent (unit 4). The eruptive foci are aligned along a NNE–SSW-trending alignment (Fig. 1), which is interpreted to represent the surface expression of a dike at depth
- The remarkably consistent chemistry of the pumices and melt inclusions (Dunbar and Kyle, 1993; Sutton et al., 1995). Dunbar and Kyle (1993) show that the pre-eruptive volatile contents varied only from 3.6 to 4.3 wt.% H_2O , with no significant systematic variations through the eruption or across major changes in eruptive style or eruption rate.

The Taupo eruption thus allows us to examine the behavior of a chemically homogeneous, crystal-poor (phenocryst abundances of 2–3.5 wt.%) rhyolitic magma which was erupted at intensities up to an order of magnitude higher than those observed in the largest late-

19th and 20th century eruptions (Table 1) This uniformity of the pre-eruptive magma allows us to interpret the great range in eruption products, eruptive styles and rates, and pyroclast characteristics in terms of purely physical influences.

The Taupo eruption products consist of 7 units (Fig. 2), yielding a 7-fold stratigraphy (Table 2), equating with 7 contrasting eruption phases (Fig. 2, Table 2). The eruption involved at least three vents on a NE–SW fissure along the eastern shoreline of Lake Taupo (Smith and Houghton, 1995) (Fig. 1). The initial phase was phreatomagmatic, forming a fine-grained fall deposit (unit 1) restricted to within 15 km of the inferred vent. Phase 2 of the eruption produced a bedded 1.6 km^3 (DRE) Plinian fall deposit (unit 2; Walker, 1981a) and minor, principally late-stage, pdc deposits. Phases 3 and 4 are represented by 1.1 and 0.8 km^3 (DRE) phreatoplinian fall deposits separated by a syn-eruptive erosional unconformity (Walker, 1981b, Smith and Houghton, 1995, Smith, 1998). Unit 3 is dm-scale bedded, rich in fine ash and dominated by highly vesicular pumice (Houghton and Wilson, 1989; Houghton et al., 2003) with a low content (<8 wt.%) of wall-rock lithics. It contains four subunits, of which subunit 3c is a distinctive well-sorted pumice lapilli bed of Plinian-style dispersal. The first subunit (3a) contains a mixture of fine ash and lapilli, whereas fine ash and accretionary lapilli dominate subunits 3b and 3d. Medial and distal exposures of unit 3 are solely of fall origin but proximal outcrops contain a significant proportion of material inferred to have been laterally emplaced by 'wet', dilute pyroclastic density currents (Smith, 1998).

Unit 4 has similar dispersal and overall grain size characteristics to unit 3 but is very different in detail. Its key characteristics are: wide dispersal yet exceedingly fine grain size, with close to 100 wt.% of the deposit finer than 1 mm (Walker, 1981b); a fine-scale laminated

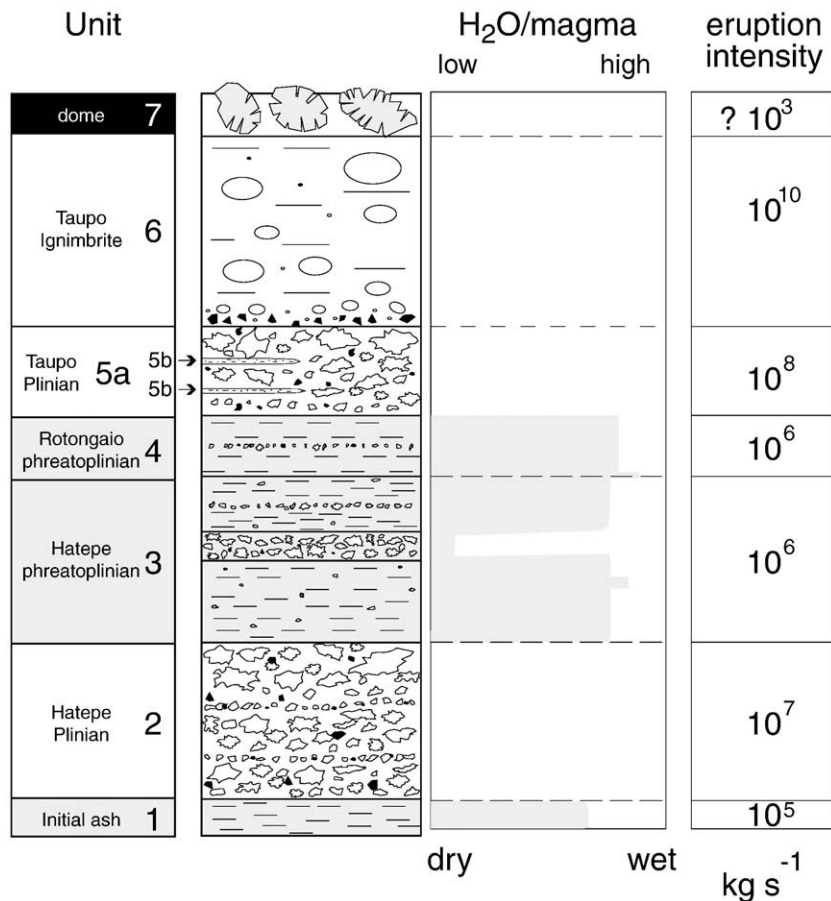


Fig. 2. Eruptive products of the 1.8 ka Taupo eruption, modified after Wilson and Walker (1985). Eruption intensity (mass eruption rate in kg/s, see Table 2) and degree of water interaction were inferred from deposit geometry and grain size characteristics. Relative thickness of deposits not to scale.

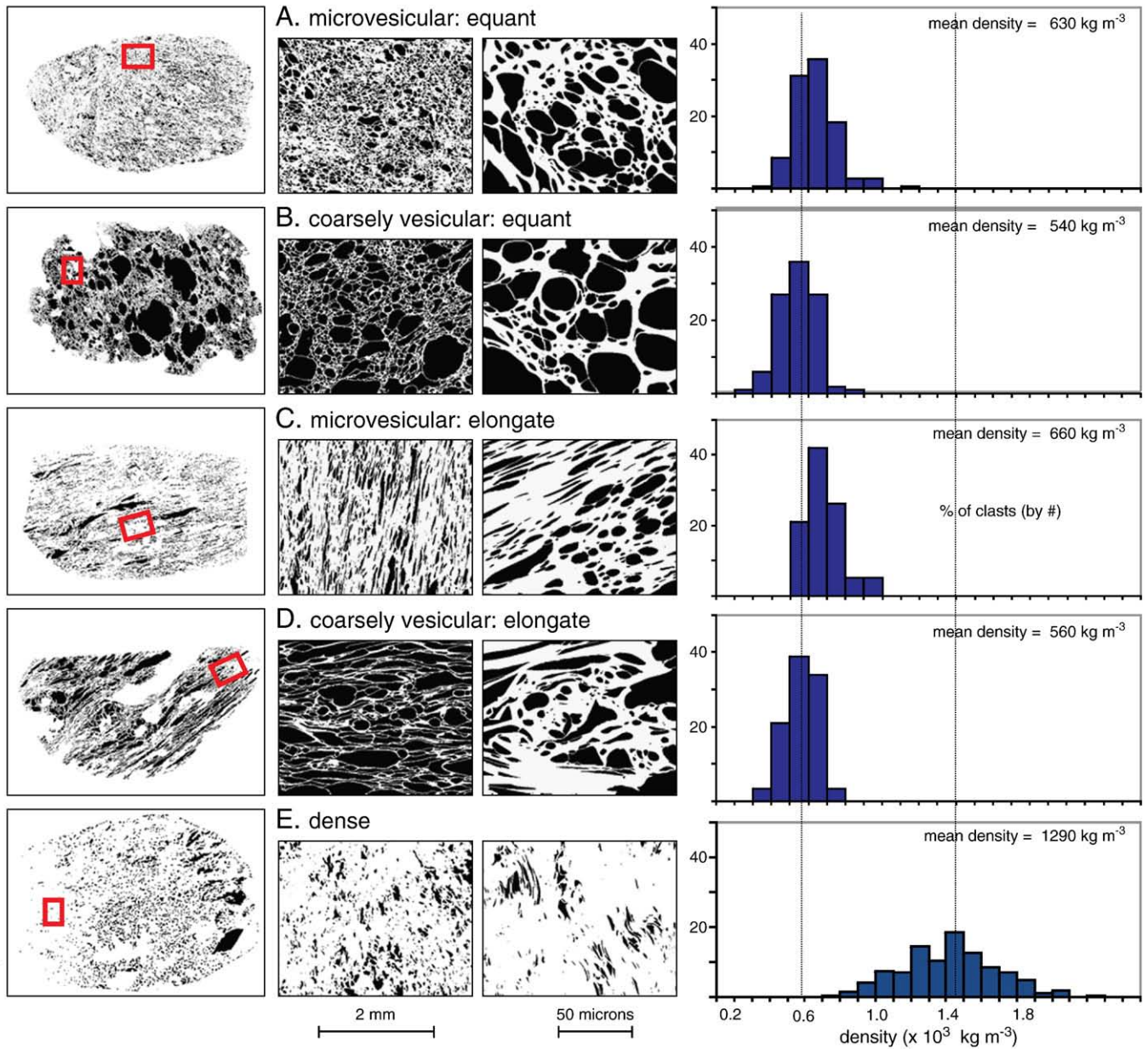


Fig. 3. Microtextures of the principal types of pumice observed in the Taupo deposits. Vesicles are shown in black and glass in white. For each clast we show one selected image at each of three magnifications: a scan of the entire thin-section, and 25× and 500× magnification SEM images.

character even in the most proximal exposures, yet a lack of lateral continuity over distances >10 m for these laminae. Unit 4 has an extremely low wall-rock lithic content, and a predominance of grey poorly to moderately vesicular juvenile clasts (Houghton and Wilson, 1989; Houghton et al., 2003). Unit 5 is the exceptionally powerful Taupo ‘ultraplinian’ fall deposit (5.8 km³ DRE: Walker, 1980), erupted coevally with at least 11 modest-volume pyroclastic flow units (shown schematically on Fig. 2 as 5b) deposited by relatively weakly energetic, concentrated pyroclastic density currents (flows, *sensu stricto*) associated with partial collapses of the Plinian plume or gentle overflow from the vent (Walker and Wilson, 1985). Explosive volcanism culminated in the generation of unit 6 (Wilson, 1985), the 12.1 km³ (DRE) highly energetically emplaced Taupo ignimbrite (Fig. 2). This deposit shows many different lithofacies, most noticeably a bipartite subdivision into layers 1 and 2 deposits attributed to deposition from the head and body of the pyroclastic density current, respectively (Wilson, 1985).

At some stage after the close of explosive volcanism, probably after an interval between several years and a few decades, rhyolitic lava domes, whose remnants are represented at the present day by the Horomatangi Reefs and Waitahanui Bank, were extruded onto the floor of the re-formed Lake Taupo. Meter to decameter-sized pumiceous blocks (‘unit 7’ here) are inferred to have spalled from the dome carapaces, floated ashore, and been incorporated in lacustrine shoreline sediments (Wilson & Walker, 1985). We have sampled this material because it provides a window into continued evolution of Taupo magma after the close of explosive eruption.

1.3. Terminology

In this paper we adopt the vesicularity classes of Houghton and Wilson (1989): *non-vesicular* (0–5 vol.% vesicles), *incipiently vesicular* (5–20 vol.%), *poorly vesicular* (20–40 vol.%), *moderately vesicular* (40–

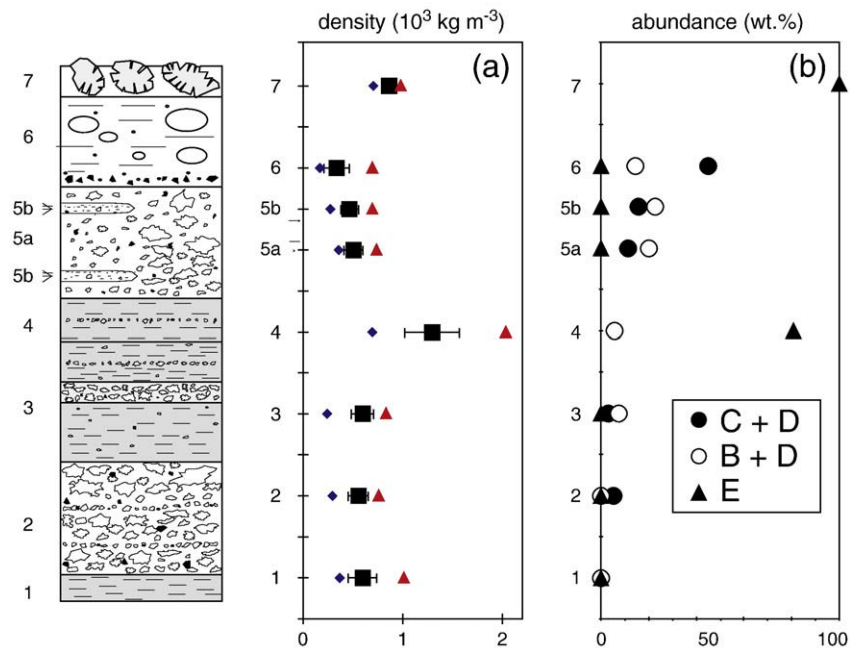


Fig. 4. Mean density values (squares) and one standard deviation (shown as error bars) for data from samples of 100 particles sampled over narrow stratigraphic intervals from the 1.8 ka deposits, together with average values calculated for the three densest (triangles) and three lightest (diamonds) clasts in each sample, plotted against stylized stratigraphic height. Number labels are from Table 2. The right-hand column plots the abundance in weight % of all elongate pumice (closed circles), all coarsely vesicular pumice (open circles) and dense clasts (closed triangles). The abundance of microvesicular clasts is equal the difference between 100 and the sum of clast types shown.

60 vol. %), *highly vesicular* (60–80 vol.%) and *extremely vesicular* (>80 vol.%). In addition, we distinguish between the phenomena of degassing (the process of formation of vesicles by exsolution of volatiles from a melt) and outgassing (the escape of the gas phase/bubbles from the host melt in the conduit).

2. Sampling and methods

The sampling strategies and techniques used in this study are outlined here and described in detail in Shea et al. (2010). Samples of at least 100 and up to 400 particles were collected over narrow vertical intervals (1–3 clasts high) for all units from the eruption. For unit 4, only one subunit was sufficiently coarse to sample for 18–32 mm clasts, and for the floated blocks (unit 7) we collected a total of 50 pieces broken in a grid pattern from a single 4-m block. These particle sets form the basis for microscopic studies.

The densities of the individual particles were measured and used as a filter to select between 3 and 7 particles with equant near-spherical vesicles that represent the mean and extreme values of density, and hence vesicularity, in each sample for microscopic examination. Vesicle numbers, shapes and abundances in these particles were quantified using a combination of images captured on petrographic and scanning electron microscopes. Typically 14 images, collected at a range of magnifications from 12.5× to 500×, were transformed to binary images (glass/crystals and vesicles), and analyzed to obtain feature areas, perimeter lengths and elongation ratios. Linear size distributions were converted to volume distributions using the stereological techniques of Sahagian and Proussevitch (1998). We applied an arbitrary lower limit of 4 μm for the measured vesicles to facilitate comparison with previous published work (Houghton et al., 2003; Adams et al., 2006a, 2006b; Carey et al., 2009). Bubble coalescence features (e.g., thinning, rupture, retraction and wrinkling of bubble walls; deformation of adjacent vesicles) are described qualitatively from the images. We have also quantified the sparse abundance of the larger crystals from the same image sets.

3. Macroscopic textures

Collections of 100 juvenile clasts from each eruption unit were divided into the five textural components and the abundances of each component. These are:

- A: white, microvesicular pumice dominated by equant bubbles of diameter, which, in SEM images, can be seen to be tens to hundreds of microns in diameter (Fig. 3a),
- B: white, coarsely vesicular pumice containing equant millimeter-sized bubbles (Fig. 3b),
- C: white, long-tube microvesicular pumice with elongate bubbles (Fig. 3c),
- D: white, long-tube coarsely vesicular pumice with elongate bubbles (Fig. 3d), and
- E: grey, dense material with sparse and deformed vesicles of varying sizes (Fig. 3e).

The volumetrically dominant textural component is type A, but all samples also contain some proportion of textural types B through E. The principal contrast between the microvesicular and coarsely vesicular pumices is that, at every magnification, the population of bubbles is markedly coarser in the latter. In hand specimen, the coarsely vesicular clasts contain large coalesced or near-coalesced bubbles either singly or as clusters where the vesicle walls are markedly thinner than in adjacent microvesicular portions of the clasts. In the clasts with elongate stretched bubbles, these fabrics persist at all magnifications but, at 500× magnification, the clasts show alternating 50 to 100 μm wide bands characterized by elongate and equant vesicles respectively (Fig. 3c, d).

All clasts in categories A through D are highly to extremely vesicular whereas the E-type clasts are generally poorly to moderately vesicular (mean vesicularity 46%, range 18–74%). There are slight differences in density/bulk vesicularity between clasts displaying textures A through D (Fig. 3). The coarsely vesicular clasts (Fig. 3b,d) have slightly lower densities than the microvesicular clasts (Fig. 3a,c) irrespective of vesicle fabric, e.g., vesicularity means (and ranges) for the clast populations

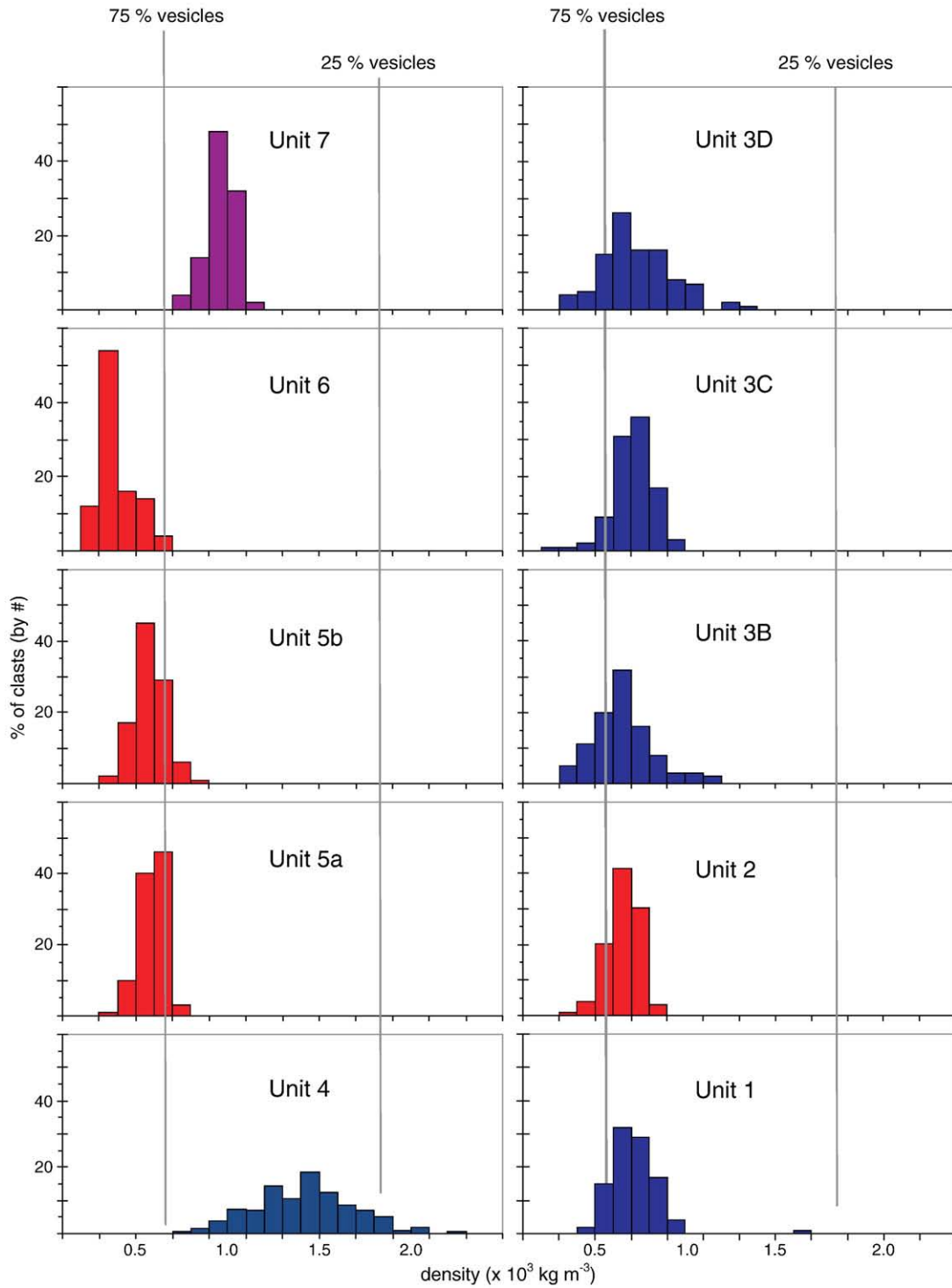


Fig. 5. Clast density histograms of units (and sub-units) of the Taupo eruption deposits. Blue histograms denote phreatomagmatic phases, red magmatic phases, and purple the closing extrusive phase of the eruption.

shown in Fig. 3 are A: 72% (58–84%), B: 77% (64–87%), C: 73% (60–78%), and D: 76% (69–84%).

White microvesicular pumice (types A and C) dominates the clast assemblages of units 1, 2 and 3 (Fig. 4). There is then a dramatic shift to a population of dense gray, poorly to moderately vesicular clasts (type E) that characterizes unit 4. To examine variations in clast type throughout the later phases of the eruption we have summed types B + D (coarsely vesicular pumice, irrespective of fabric; labeled ‘coalesced’ in Fig. 4b) and C + D (long tube pumice independent of bubble size; labeled

‘sheared’ in Fig. 4b). Fig. 4b shows that the main phases of the eruption (units 5 and 6), particularly unit 6, are marked by an increase in the proportion of tube (sheared) pumices, as well as an increase in the proportion of highly expanded (coalesced) pumice clasts. Unit 7, like unit 4, is dominated by grey clasts that have a restricted vesicularity range of 58–73%. The individual unit 7 blocks are cut by dm-wide zones up to 4 m long characterized by clusters of coalesced 1–3 cm diameter vesicles. The samples collected here are representative of the finely vesicular material between these zones. All rocks contain 2 to 3.5 wt.% of

1–3 mm phenocrysts, principally plagioclase and quartz. Microphenocrysts occur only in the floated blocks of unit 7, and sparse microlites in unit 4.

4. Density and bulk vesicularity

The new density data are consistent with the earlier study of Houghton and Wilson (1989), which showed that the two Plinian deposits (units 2 and 5a) have the narrowest density/vesicularity ranges (Figs. 4a and 5) and that the ‘ultraplinian’ unit 5a contains pumices with a lower mean density and slightly narrower range than the Plinian unit 2. Here we show that the lowest density clasts are stretched long tube pumice (clast types C and D). Two of the three phreatomagmatic deposits (units 1 and 3) also contain highly vesicular pumices but also have a small tail of denser clasts (800 to 1100 kg m⁻³; Fig. 5), equivalent to vesicularities of 53 to 66%. The least dense, most vesicular clasts (density 120–300 kg m⁻³; vesicularity 85–95%) occur in the samples from the two ignimbrite units (5b and 6 in Figs. 4a and 5). The densest clasts and widest density ranges occur in phreatoplinian unit 4, where the density mean of 1200 kg m⁻³ and range of 500 to 2100 kg m⁻³ is markedly different from all other units (Figs. 4a and 5). Individual fragments collected from late-stage grey pumiceous blocks of unit 7 have a more limited density range (650 to 1000 kg m⁻³), equivalent to vesicularities of 58 to 73% (Figs. 4a and 5). Vesicularity data can also be expressed in terms of the ratio V_G/V_L , the volume of vesicles (gas) to that of glass (liquid), after Gardner et al. (1996), as a more sensitive measure of relative gas volume. There is a strong correlation between V_G/V_L and estimated/inferred mass discharge rate (MDR, or intensity) for both modal and minimum vesicularity clasts throughout the eruption (Fig. 6). In particular for unit 6 it appears that, for high rates of bubble nucleation the melt also experienced more opportunity for bubble deformation along conduit margins (reflected in the high abundance of type C tube pumice: Fig. 4) and, possibly, more opportunity for syn-eruptive expansion (related to decreased rates of heat loss in the relatively dense, collapsing eruption column).

5. Microscopic textures

Figs. 7 and 8 show SEM images from clasts representative of the modal (middle), maximum (left) and minimum (right) vesicularities in each sample chosen to represent a unit or subunit. There is a wide range of microtextures present in these clasts, which show significantly more diversity than one might infer from the density data and the macroscopic textures alone. A striking feature is that many clasts are internally heterogeneous, in terms of vesicle distribution, size, shape, and elongation, containing domains that may correspond to any one of textures A through D described above. This small-scale heterogeneity is common in silicic pumice (e.g., Klug et al., 2002) and in part reflects strain localization in these highly vesicular magmas (Wright and Weinberg, 2009).

Clasts from unit 1 are characterised by a population of relatively mature coarse vesicles with complex shapes showing ample evidence for coalescence but little sign of flattening and shearing or bubble relaxation (Fig. 7a,b,c). In pumices that represent the mean and highest densities, the largest vesicles have a heterogeneous distribution in clusters or weakly defined bands and possess colloform to irregular curvilinear shapes (Fig. 7b,c). Low-density pumice clasts have abundant large (0.5 to 1.5 mm) vesicles that form networks of interpenetrating bubbles with thin and often complexly deformed glass walls (Fig. 7a). Vesicles in all three clasts show a wide range of shapes from spherical to complexly contorted (Fig. 7) with the simpler forms typifying the smaller vesicles (<50 μm).

The unit 2 pumices contain smaller vesicles than unit 1 clasts (Fig. 7d,e,f) while still preserving evidence for bubble coalescence (retracted walls, convolute and colloform shapes, etc.). In particular

the largest vesicles show complex curvilinear shapes and cluster into mm-scale groups (Fig. 7d). Smaller vesicles are typically simpler in form (spherical to ovoid), although the mean density clast shows evidence of shear localization (e.g., Fig. 7e). There is markedly less deformation of vesicles in the low-density pumice.

We have processed two samples from unit 3, one from subunit 3C (Fig. 7g,h,i), the lapilli-rich bed in the centre of the unit (in grain size similar to the dry unit 2 Plinian fall deposit at the same distance from vent), and one from an ash-rich unit within subunit 3D (Fig. 7j,k,l). In this way we hoped to contrast ‘drier’ and ‘wetter’ end-members of phreatoplinian volcanism. These six unit 3 pumices are perhaps the most diverse grouping that we studied. Two clasts show marked stretching of vesicles of all sizes leading to a pervasive long-tube fabric (Fig. 7g,l); two others show shear localization (Fig. 7i,k) and two are characterised by densely packed, equant vesicles with complex shapes reflecting the influence of interaction and coalescence between bubbles (Fig. 7h,j). There is, however, no correlation between the degree of stretching and clast vesicularity, as the two long-tube pumices represent the extremes of unit 3 vesicularity at 58% and 93%. This variation probably reflects different amounts of bubble wall collapse associated with the stretching (e.g., Wright et al., 2006).

We analysed four clasts from unit 4 (Fig. 9) in recognition of the broadly bimodal distribution of clast densities and hence vesicularities, although this distribution can only be quantified for the one coarser horizon. The unit 4 clasts are highly distinctive, with few features in common with the pumices of the immediately over- and under-lying units. Vesicles have glass walls with thicknesses that increase with increasing density (Fig. 9). A striking feature is the occurrence of mm-long zones of larger (200–500 μm) bubbles with complex indented walls surrounded by dense zones with 10–30 μm vesicles (Fig. 9b,c). Even widely spaced vesicles have mostly sheared complex curvilinear and flamme-like shapes (Fig. 9), especially in the high-density clast (Fig. 9d). These textures are very similar to those observed in obsidian flows (e.g., Fink et al., 1992; Rust and Cashman, 2004; Adams et al., 2006b) where originally vesicular magma has densified because of bubble collapse during flow.

The three clasts from the Plinian fall deposit of unit 5a show a wide range of vesicle sizes with the larger bubbles formed by coalescence (Fig. 8a, b, c). The high density clast shows localization of shear, with clusters of large equant vesicles surrounded by a more finely vesicular, and more deformed, material (Fig. 8c). Fabrics are much less conspicuous in the pumice clasts from the coeval ignimbrite of unit 5b (Fig. 8d,e,f), where the bubbles are larger (more expanded) than in the unit 5a Plinian counterparts. Large vesicles are equant with colloform shapes and abundant retracted filaments that indicate large bubble formation by coalescence of numerous millimeter-sized vesicles. The low-density pumice contains striking clusters of large

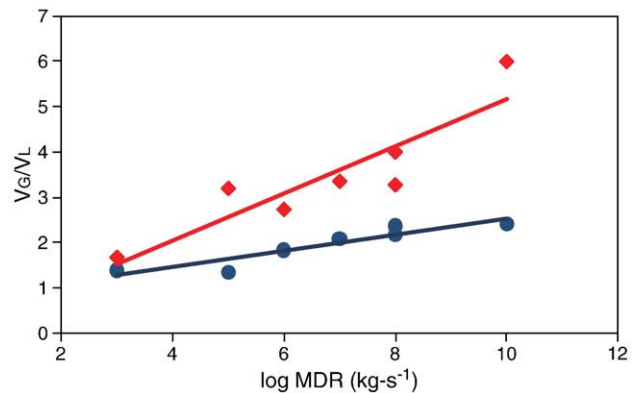


Fig. 6. A plot of V_G/V_L vs. Log eruption intensity (MDR: mass eruption rate in kg/s) for modal (red diamonds) and minimum (black circles) vesicularity clasts from the Taupo eruption.

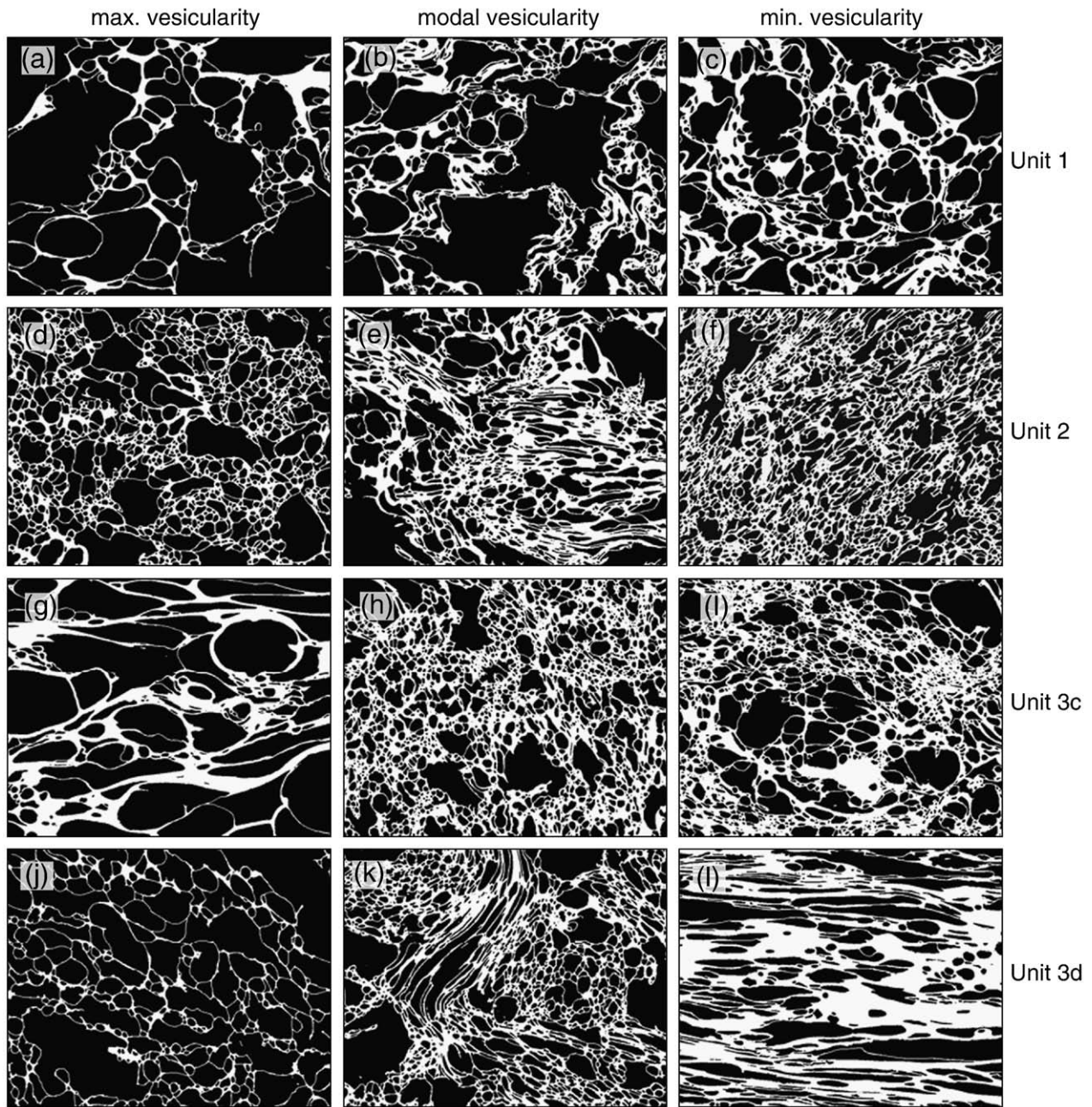


Fig. 7. Selected binary images of pumices from the lower stratigraphic units of the Taupo sequence. Vesicles are black, glass (+ minor phenocrysts and microlites) are white. Most images are at 75 \times magnification but h is at 100 \times . Width of the field of view is 900 μm for 75 \times images and 670 μm for the 100 \times image.

coalesced vesicles surrounded by small bubbles with flat polygonal walls (Fig. 8d).

The sample of unit 6 was taken from a fines-poor layer 1 deposit. All three pumice clasts have closely packed assemblages of relatively equant vesicles (Fig. 8g,h,i). The mean-density pumice has sparse large (mm-sized) vesicles set in a network of smaller polygonal to complex curvilinear bubbles, with thin glass walls (Fig. 8h). The high-density pumice has a similar texture with thicker walls (Fig. 8i). The low-density pumice (Fig. 8g) is a polydispersive network of relatively large bubbles separated by remarkably thin walls.

The three fragments examined from the dome-derived floating blocks are uniform in texture (Fig. 8j,k,l) with large, highly irregular but equant vesicles surrounded by regions of denser glass that contains flattened vesicles that appear to have partially collapsed.

6. Quantifying vesicle textures

6.1. Vesicle number densities

Simple number counts of vesicles are a potentially powerful tool to understand rates of magma ascent because of the relationship between number density and decompression rate observed in laboratory experiments on rhyolitic melts (Mourtada-Bonnefoi and Laporte, 1999, 2004; Mangan & Sisson, 2000; Mangan et al., 2004; Toramaru, 2006). The Taupo magma, being phenocryst-poor, is a near-ideal natural system to compare with the experimental data from crystal-free rhyolitic melts to derive estimates of ascent rates. We report number densities in two forms here: firstly, corrected for the presence of phenocrysts (N_v) and secondly for the presence of

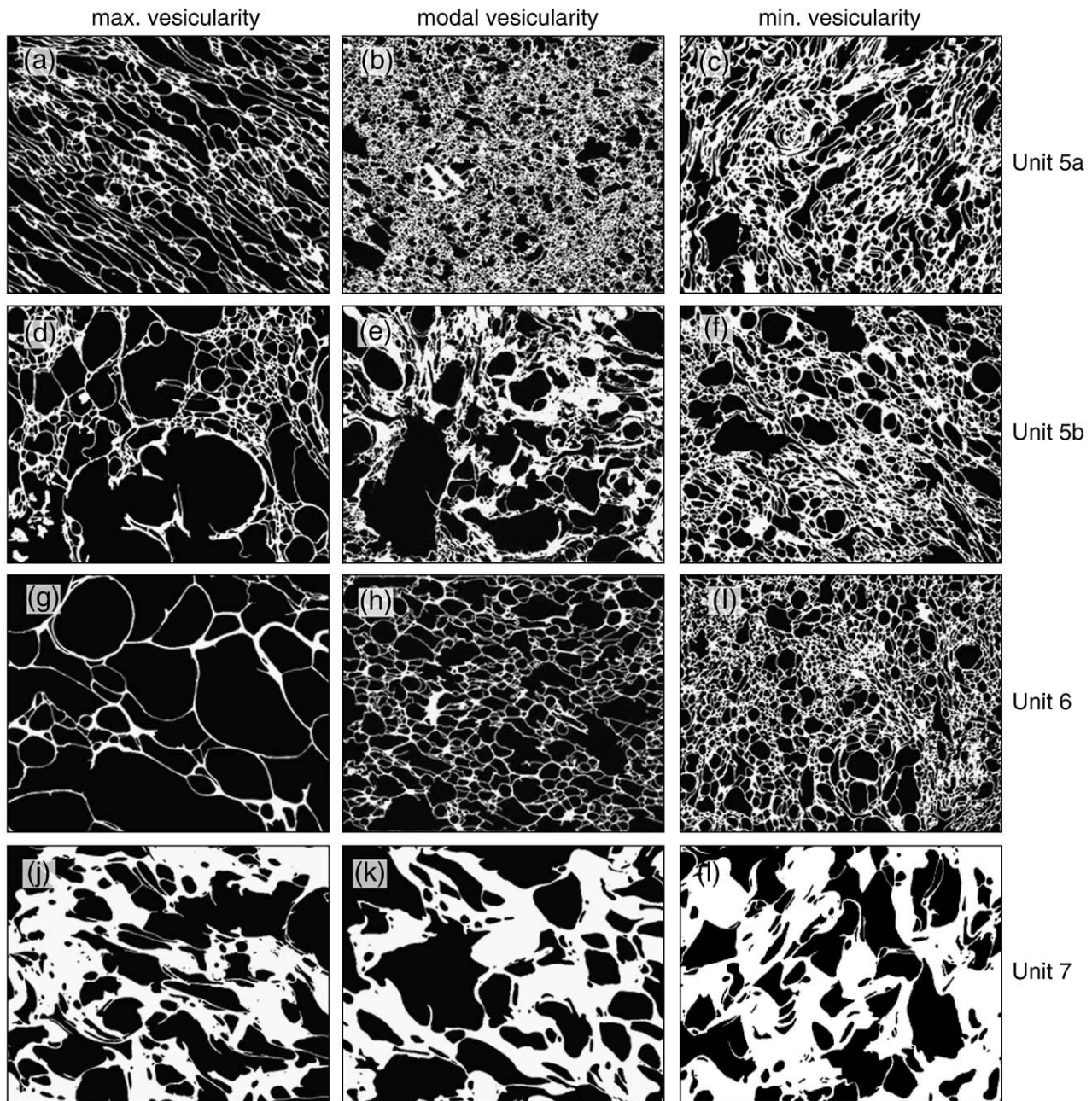


Fig. 8. Selected binary images of pumices from the upper stratigraphic units of the Taupo sequence. Vesicles are black, glass (+ minor phenocrysts and microlites) are white. Most images are 75 \times magnification but a and b are at 50 \times . Width of the field of view is 900 μm for 75 \times images and 1340 μm for the two 50 \times images.

both phenocrysts and bubbles (N_v^m) respectively. The former is more widely used but, as Klug et al. (2002) point out, underestimates the abundance of bubbles in highly vesicular materials. For this reason the comparisons between phases of this eruption made below are done in terms of N_v^m .

There is a persistence of N_v^m values of $10^{8.5}$ to $10^{9.5} \text{ cm}^{-3}$ throughout much of the Taupo eruptive sequence (Table 3) despite clear textural evidence for diversity in bubble size distributions and bubble shapes, and for modification of number densities due to coalescence. These values are similar to those observed in pumice from other Plinian eruption deposits (e.g., Klug and Cashman, 1994; Klug et al., 2002; Gurioli et al., 2005; Adams et al., 2006b). Measured melt-corrected number densities are substantially higher than those produced in experiments where the only volatile phase is H_2O (e.g., Mangan and Sisson, 2000; Mourtada-Bonnefoi and Mader, 2004), and overlap or are

slightly higher than those produced by homogeneous nucleation driven by rapid ($>1 \text{ MPa/s}$) decompression of rhyolitic melt that contains a mixed $\text{H}_2\text{O}-\text{CO}_2$ volatile phase (Mourtada-Bonnefoi and Laporte, 2002). Surprisingly, pumice number densities appear to be independent of the estimated MDR, both within the Taupo eruption and among rhyolitic Plinian deposits (Fig. 10). This insensitivity to mass eruption rate may reflect similar decompression rates for all eruptions (with MDR controlled primarily by vent size) and/or limits to the kinetics of bubble nucleation in rhyolitic melts.

6.2. Vesicle sizes

In magmas that have not been affected by vesicle collapse, minimum vesicle size is a measure of the extent to which bubbles continued to expand after nucleation ceased. Vesicle volume distributions for pumice

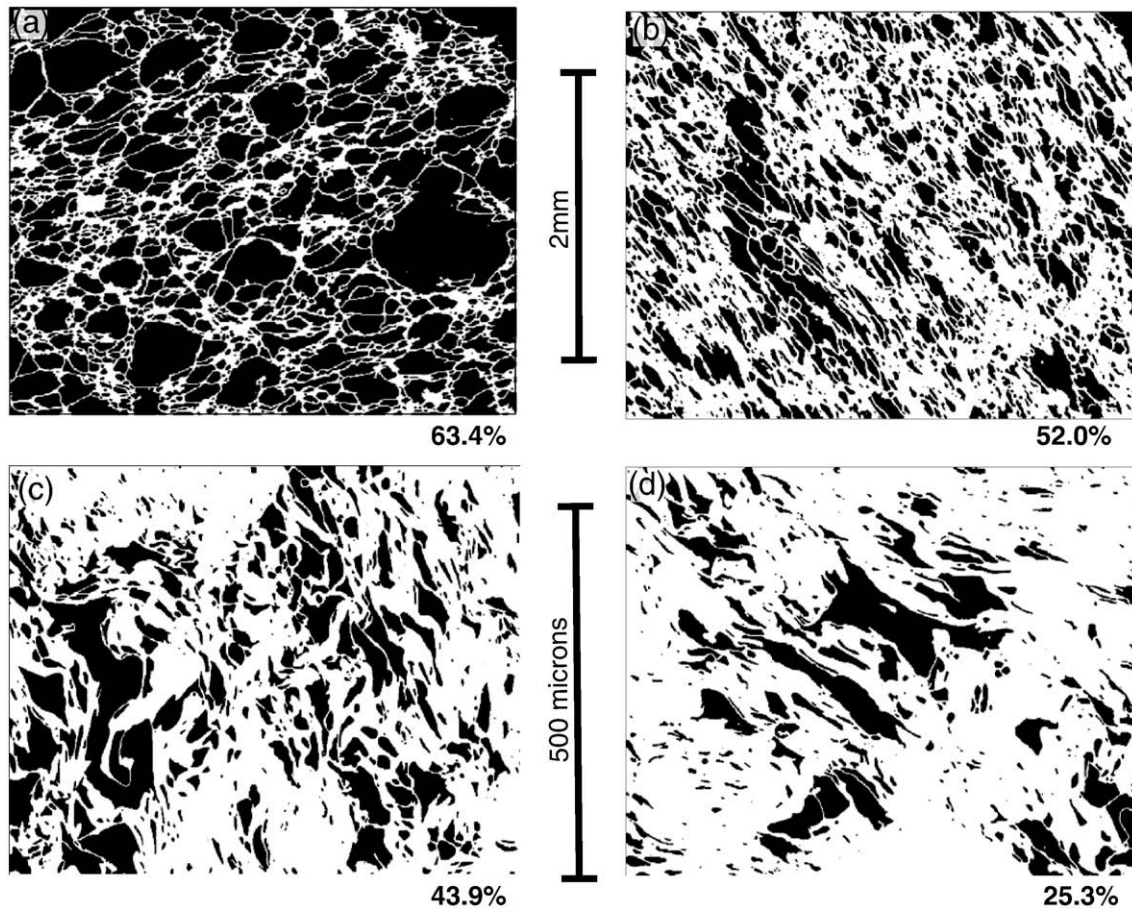


Fig. 9. Binary images of clasts from unit 4 showing complex textures associated with outgassing and collapse of vesicles. The images show progressive thickening of the glass walls with decreasing vesicularity from a to d. In b, c, and d, domains of larger, complexly deformed vesicles are surrounded by regions with few vesicles and thick glass walls. Vesicularity listed as vol.%.

from Taupo Plinian and phreatoplinian deposits show a mode at 30–40 μm (particularly well developed in Units 3d and 5a; Fig. 11; Table 3). The prevalence of this size mode is required by the high number density and indicates that bubble growth was limited because of neighboring bubbles (e.g., Sparks, 1978). In contrast, pumice clasts from the two ignimbrites (units 5b and 6) contain clusters of large (1–8 mm) vesicles. Together with the high vesicularities and very thin bubble walls in these samples, this texture indicates substantial post-nucleation expansion of these clasts and accompanying bubble coalescence. We speculate these highly inflated clasts are the product of both vent-widening, which permitted unconstrained expansion, and the high heat content of the density current. However, even these Taupo samples are less obviously polymodal than for many silicic Plinian tephra (Sparks and Brazier, 1982; Whitham and Sparks, 1986; Orsi et al., 1992; Klug and Cashman, 1994; Klug et al., 2002).

Pumice clasts from units 1, 4 and 7 show distinctive textural characteristics that provide clues about their origins. Clasts from units 1 and 7 typically lack a small vesicle (<50 μm) mode and, instead, exhibit a dominant vesicle size of 250–400 μm (Table 3). In unit 7, the moderate vesicularities and evidence for bubble collapse suggest that small bubbles were lost because of partial densification of the dome lavas. In contrast, unit 1 samples have thin bubble walls and high vesicularities that indicate extensive bubble expansion, perhaps related to slower ascent of the vanguard magma. Large vesicles are totally absent in the four clasts from unit 4. These clasts have low to moderate vesicularities, single vesicle modes at $\leq 100 \mu\text{m}$, and extensive textural evidence of bubble deformation and collapse that records non-explosive outgassing prior to eruption.

Cumulative number densities for the Taupo data obey a power law relationship for all vesicles larger than 10 μm , with an exponential decay value of approximately -3.2 . This value is typical of Plinian pumice samples (e.g., Klug et al., 2002; Shea et al., 2010) and indicates that small vesicles comprise most of the vesicle volume. Power law distributions are commonly interpreted to reflect continuous bubble nucleation during magma ascent (e.g., Blower et al., 2002); power law exponents > 3 may be characteristic of rapid bubble nucleation at high supersaturation.

6.3. Evolution of textural types

The type A, equant microvesicular clasts follow a tight trend with high vesicle number densities but relatively low V_G/V_L (Fig. 12). Coarsely vesicular type B clasts, with coalescence features, have marked lower number densities, despite generally higher V_G/V_L . Pumices with long tube fabrics (types C and D) have similar number densities to types A and B and the highest V_G/V_L , reflecting packing efficiency. The type E, dense clasts analysed from units 4 and 7 show two trends on Fig. 12. The floated pumice blocks of Unit 7 have very low vesicle number densities but only slightly lower V_G/V_L than the pyroclastic pumices. Dense clasts from unit 4 define a linear trend of sharply declining number density and V_G/V_L .

We compare vesicularity for the Taupo samples in Table 4 and Fig. 10, to the products of three well documented but smaller historical eruptions of silicic magma (Vesuvius 79, Askja 1875, Novarupta 1912), where vesicularity data was obtained using the same techniques and 4 μm size-cut-off that were applied to the Taupo samples. The data show a broad overlap for the four eruptions but the highest number

Table 3
Vesicularity characteristics of the analysed Taupo clasts. N_v , number density of vesicles, corrected to allow for presence of phenocrysts; N_v^m , number density of vesicles, corrected to allow for presence of phenocrysts and vesicles.

Clast	Unit	Vesic class	Vesic (%)	V_g/V_1	N_v (cm^{-3})	N_v^m (cm^{-3})	Vol-based median (mm)	1° mode (mm)	2° mode (mm)	Coarse 3° mode (mm)
50106	1	high	85	5.7	1.03E+07	6.89E+07	0.600	0.320		
50124	1	mode	76	3.1	6.34E+07	2.60E+08	0.120	0.250		
50138	1	low	65	1.9	1.33E+08	3.84E+08	0.100	0.032	0.64	
20202	2	high	85	5.6	1.97E+08	1.30E+09	0.045	0.032		
20241	2	mode	76	3.2	1.65E+08	6.96E+08	0.100	0.100	1.60	
20206	2	low	60	1.5	2.48E+08	6.19E+08	0.075	0.032		
90204	3C	high	93	13.7	1.82E+08	2.67E+09	0.075	0.400	1.26	
90206	3C	mode	75	3.0	8.80E+08	3.52E+09	0.040	0.016		
90253	3C	low	65	1.8	1.75E+08	4.97E+08	0.040	0.032		
90102	3D	high	90	8.5	6.82E+07	6.49E+08	0.100	0.100		
90105	3D	mode	75	3.0	2.36E+08	9.38E+08	0.040	0.032		
90106	3D	low	58	1.4	2.15E+08	5.09E+08	0.040	0.032		
70115	4	high	63	1.7	1.18E+08	3.23E+08	0.070	0.100		
70111	4	mode 1	44	0.8	1.95E+08	3.47E+08	0.028	0.032		
70101	4	mode 2	52	1.1	1.20E+08	2.49E+08	0.050	0.100		
70121	4	low	25	0.3	8.94E+07	1.20E+08	0.025	0.032		
10102	5A	high	88	7.1	1.97E+08	1.59E+09	0.043	0.032		
10105	5A	mode	75	3.0	7.65E+08	3.06E+09	0.038	0.025	0.80	
10103	5A	mode	79	3.8	2.11E+08	1.01E+09		0.032		
10120	5A	low	71	2.5	1.85E+08	6.46E+08	0.040	0.160		
80155	5B	high	90	8.8	1.94E+08	1.91E+09	0.110	0.032	0.16	6.38
80197	5B	mode	81	4.3	9.19E+08	4.84E+09	0.160	0.120		3.16
80192	5B	mode	81	4.3	2.81E+08	1.48E+09	0.050	0.032	0.16	
80174	5B	low	69	2.2	1.60E+09	5.15E+09	0.025	0.025		
30256	6	high	93	14.2	3.54E+08	5.36E+09	0.030	0.032		
30243	6	mode	87	6.7	2.97E+07	2.28E+08	0.080	0.080		
30206	6	mode	89	7.9	7.52E+07	6.72E+08	0.075	0.032	0.08	2.01
30236	6	low	76	3.1	2.92E+06	1.20E+07	0.080	0.032		
60118	7	high	73	2.7	1.40E+07	5.18E+07	0.180	0.320		
60143	7	mode	64	1.8	6.77E+06	1.89E+07	0.230	0.400		
60140	7	low	58	1.4	2.35E+07	5.94E+07		0.250		2.01

densities (greater than $2 \times 10^9 \text{ cm}^{-3}$, and at relatively low V_g/V_1 values) are attained in a subset of microvesicular Taupo clasts, associated with units 5 and 6. This is compatible with high ascent rates that can be inferred (Toramaru, 2006) for the phases of these eruptions.

7. Interpretation of vesicularity data

7.1. Vesicle size and volume distributions

Theory developed for the interpretation of crystal size distributions (Marsh, 1988, Cashman, 1992) has been applied to vesicle populations (Toramaru, 1990, Cashman and Mangan, 1994, Klug and Cashman, 1994, Mangan and Cashman, 1996). Vesicle size distributions (VSDs) for many Taupo clasts do not follow the linear trends that are predicted to equate with steady state nucleation and growth, almost certainly due to non-steady-state bubble growth (Blower et al., 2002), the role of coalescence (see Figs. 3 and 4), and mass balance constraints (Klug et al., 2002). Data from the smallest size classes are virtually identical for all clasts suggesting that the processes of bubble nucleation and early growth were basically similar throughout the eruption. Mangan et al. (2004) suggest that in rhyolitic melts with low crystal contents, high surface tension favors late-stage homogeneous bubble nucleation, generating high bubble number densities.

The number densities seen in the Taupo pumices are not attained in laboratory simulations, however, for rhyolitic melts under conditions of steady decompression (or ascent) rate, where measured values are typically one to two orders of magnitude lower (Gardner, 2007). This discrepancy between natural systems and analogue laboratory experiments has led researchers to suggest that high number densities in natural samples reflect a second late-stage, disequilibrium nucleation event in the shallow conduit (Mourtada-Bonnefoi and Mader, 2004; Cluzel et al., 2008). In this model a relatively small number of bubbles

first nucleate in the lower conduit, then rapid ascent and extreme decompression rates near the fragmentation surface trigger a second nucleation event producing a large subpopulation of small bubbles with high ΔP favoring rapid ascent and fragmentation (Toramaru, 1995; Cluzel et al., 2008). Under these circumstances we might predict bimodal size distributions, as have been recorded for the 1980 St Helens, 1912 Novarupta and Mt Mazama eruptions (Klug et al., 2002; Adams et al., 2006b).

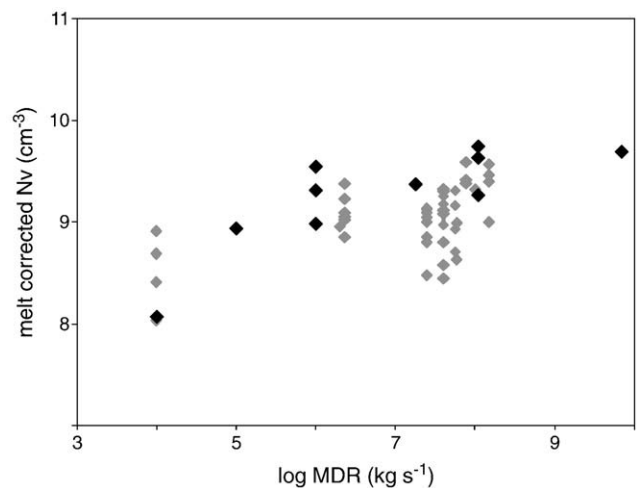


Fig. 10. Plot of mass discharge rate versus vesicle number density (N_v) for modal pumices from well constrained Plinian and phreatoplinian eruptions. Modal Taupo data in black diamonds; data from other Plinian eruptions in gray diamonds (Klug and Cashman, 1994; Polacci et al., 2001; Klug et al., 2002; Gurioli et al., 2005; Adams et al., 2006a; Carey et al., 2009).

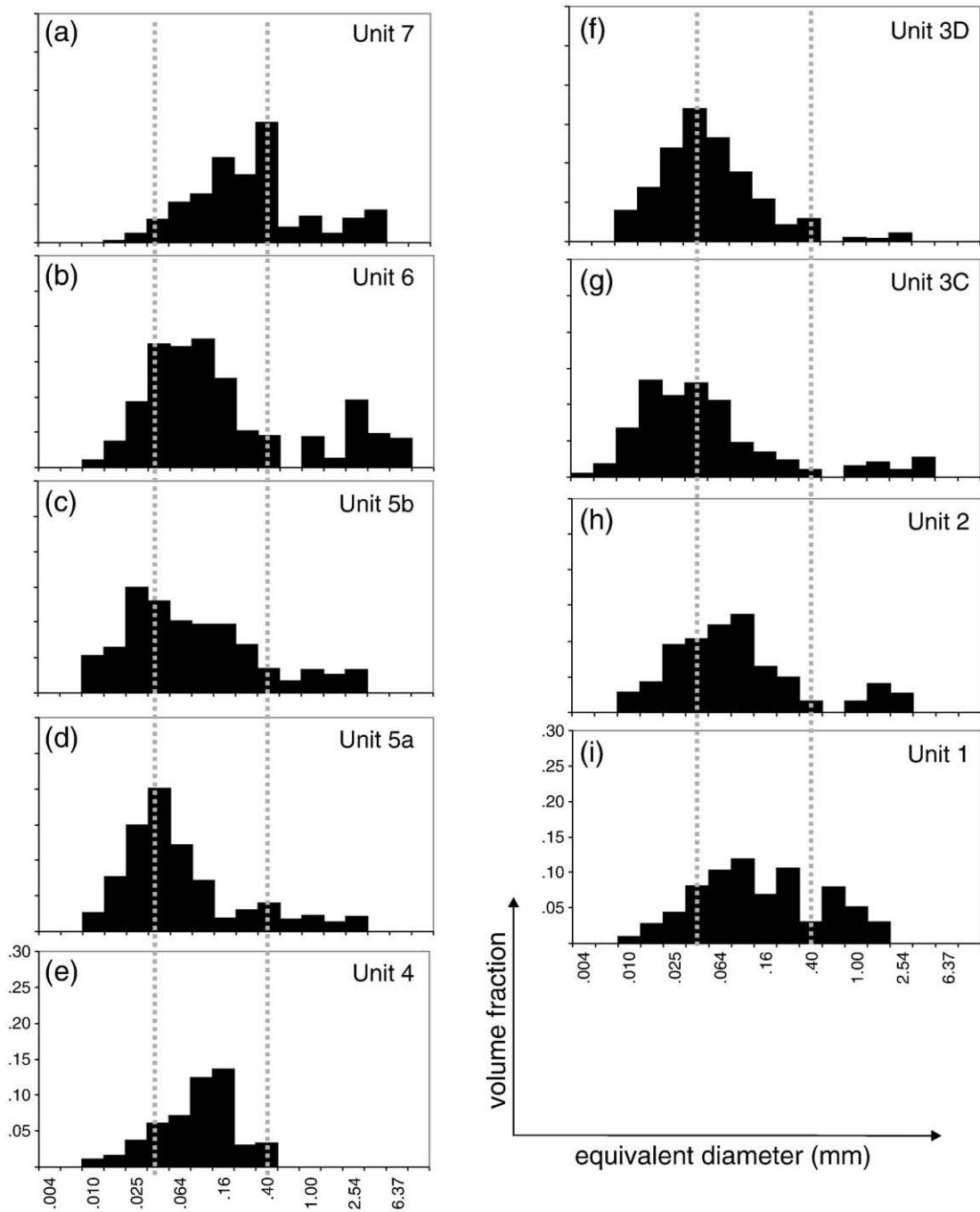


Fig. 11. Volume distribution of vesicles in the mean-density clasts from the Taupo eruption sequence. The volume distribution of six clasts from different units/subunits have modes at 30–40 μm . The 3 remaining histograms (units 1, 4 and 7) show distributions skewed to coarser vesicles, suggesting that nucleation appears to have ceased prior to the end of bubble growth and (in the cases of unit 4) collapse.

7.2. The significance of microtextural diversity between units

We can divide the vesicle textures present in clast populations from the Taupo eruption into four categories:

- (i) Very high bubble number densities and small vesicles (type A and C clasts, typical of units 2, 3, 5, 6),
- (ii) Moderately high number densities and moderate to large bubbles (e.g., unit 1 and also type B and D clasts in other units),
- (iii) Comparatively low number densities with widely spaced bubbles, often showing shearing and collapse textures (type E clasts in unit 4)

- (iv) Moderate number density and dominantly large complex-shaped vesicles (e.g., type E blocks, Unit 7).

The microvesicular clasts of type (i), which characterize all the intense phases of the eruption, represent the rapid and late nucleation of bubbles in rapidly ascending melt undergoing disequilibrium degassing. Gardner (2007) suggests that bubble number densities in rhyolitic melts erupted under Plinian conditions reflect ascent conditions and are not significantly overprinted by coalescence. If this is so, then the microvesicular clasts that predominate in units 2, 3, 5, and 6 at Taupo reflect conditions of exceptionally rapid ascent of magma, precluding significant coalescence of bubbles and culminating in the extremely powerful 5th and 6th phases

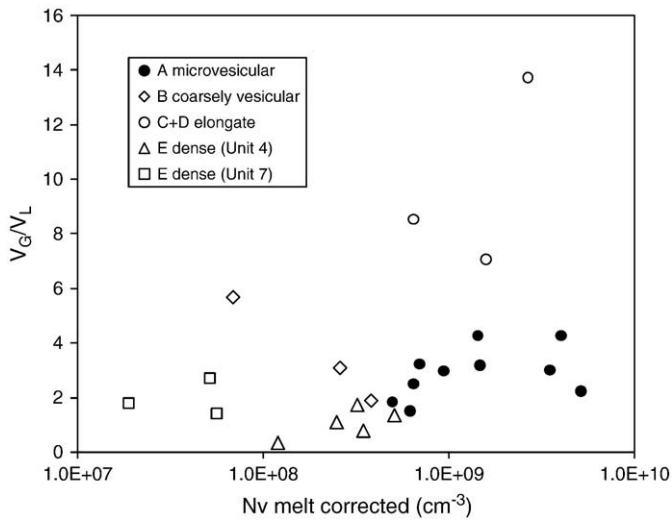


Fig. 12. Plot comparing uncorrected vesicle number density (V_n) and V_g/V_1 ratios for pumices representative of different clast textures. The highest number densities are displayed by the microvesicular type A pumices, coarsely vesicular type B pumices have lower number densities and similar or higher V_g/V_1 ratios. The highest vesicularities are represented by the elongate, long-tube pumices. The dense clasts show two contrasting trends of decreased number densities and vesicularities indicative of bubble coalescence and collapse.

of this eruption. In contrast, we suggest that clasts seen in Unit 1 (type (ii) above) develop by an overprinting of coalescence on formerly microvesicular textures. The timing of its development and overprinting is critical to understanding ascent processes – we would argue that this occurred prior to fragmentation and was a consequence of the relatively slow shallow ascent of the Unit 1 magma during the process of establishing the conduit system beneath the Taupo vents.

In unit 4 clasts, even widely spaced vesicles have mostly complex curvilinear shapes reflecting a history of extensive bubble interaction and coalescence followed by total collapse of all except the larger bubbles. However bubble number densities are still relatively high. A striking feature of the Unit 4 clasts is the diversity of textures suggesting contrasting degassing histories on very small length scales in the conduit, implying a very complex pattern for shallow-level degassing processes. We interpret this data in terms of a two-stage history of first rapid and comparatively uniform ascent, permitting late nucleation of large numbers of vesicles, and subsequent extended holding at relatively shallow level, permitting bubble coalescence and variable degrees of onset of permeability and outgassing. We believe this was possible due to ascent of the melt under a 'blind' northern portion of the feeder dike beneath the Taupo vents. The data presented by Smith and Houghton (1995), suggesting that unit 4 erupted from a newly formed vent(s) well northeast of the vent(s) responsible for units 1–3, is strong

support for the option that this portion of the Taupo magma partially outgassed under this northern vent, prior to and during its explosive disruption by a succession of many widely spaced discrete explosions. In contrast, the relatively uniform vesicle and crystal textures of the Unit 7 pumiceous dome-derived blocks is more suggestive of ascent and eruption under equilibrium conditions during which microphenocrysts could form and bubbles underwent extended coalescence.

7.3. Role of post-fragmentation expansion of bubbles at Taupo

There is only limited evidence for post-fragmentation expansion of vesicles in the Taupo pyroclasts, and this is restricted to larger clasts in the two ignimbrites. All other Taupo pyroclasts lack rinds with bubble populations markedly finer than clast interiors. In all these respects, the Taupo bubble populations are significantly different from their 18 May 1980 St Helens equivalents, where Klug and Cashman (1994) show evidence for continued vesicle development in the eruption plume.

7.4. Contrasting ascent histories and eruption processes

The Taupo samples are characterized by high vesicle number densities, even when significantly overprinted by bubble coalescence and/or collapse (e.g., units 4 and 7). This is strong indication that conditions of bubble nucleation remained similar throughout the eruption. However the diversity of microtextures frozen into the pyroclasts is an indication of marked divergence in the later histories of bubble growth and coalescence, and in some cases deformation and collapse. Below we explore how the textures could be used to build a picture of the influences modulating the Taupo eruption.

The succession of textural changes in the pyroclasts cannot be reproduced by simply changing ascent conditions at a single vent or by shifting vent position but only by a combination of these modulating influences. We propose the following sequence of events based on evidence presented here:

Unit 1 was erupted via a newly established conduit and the textural signature of relatively lower vesicle number density, relaxed bubble shapes and large vesicle sizes is commensurate with slow, steady ascent of the initial magma under conditions which permitted extensive interaction of actively vesiculating melt with the waters of Lake Taupo (Fig. 13a).

Unit 2 is the product of the most stable period of sustained eruption at Taupo. Its lack of obvious internal bedding, the absence of intercalated pyroclastic density currents, and its moderate yet near-constant grain size are consistent with a stable Plinian plume and moderate mass discharge rates. We suggest that water was denied access to the vent probably as a result of construction of a tuff ring or cone (Fig. 13b) during unit 1 times. However unit 2 contains 0.18 km³ of wall rock (Walker, 1981a). We propose that the vent was progressively widened as a

Table 4

Comparison of characteristics of pumice/juvenile clasts from the Taupo eruption with those of smaller, historical silicic eruptions.

Eruption + phase	Vesicularity range (%)	Vesicularity mean (%)	V_g/V_1	Nv^m (mm ⁻³)	Mass discharge rate (kgs ⁻¹)	
Taupo unit 2	68–87	76	2.1–6.9	0.6–1 E+09	E+07	This paper
Taupo unit 3	65–90	75	1.8–8.5	0.5–4 E+09	E+06	
Taupo unit 4	14–70	45	0.2–2.4	1–3 E+08	E+06	
Taupo unit 5	68–85	79	2.2–5.6	0.6–3 E+09	E+08	
Taupo unit 6	70–88	80	2.4–13.1	0.1–5 E+09	E+10	
Askja Unit B	74–93	85	2.8–13.3	9 E+08	E+06	
Askja Unit C1	81–93	84	4.3–13.3	1–2 E+09	E+07	
Askja Unit C2	53–92	86	1.1–11.5	1–2 E+09	E+06	
Askja Unit D	69–89	87	2.2–8.1	3–14 E+09	E+07	
Novarupta epi II	68–86	75	1.8–6.3	0.4–1 E+09	E+07	Adams et al. (2006b)
Novarupta epi III	60–84	77	1.5–5.4	0.3–2 E+09	E+07	
Vesuvius EU2	68–86	78	2.1–6.1	2–4 E+09	8 E+07	Gurioli et al. (2005)
Vesuvius EU3b	50–78	65	1.0–3.5	0.2–2 E+09	1 E+08	
Vesuvius EU3t	55–85	71	1.2–5.7	2–4 E+09	1 E+08	
Vesuvius EU4	40–85	73	0.7–5.7	1–2 E+09	4 E+09	

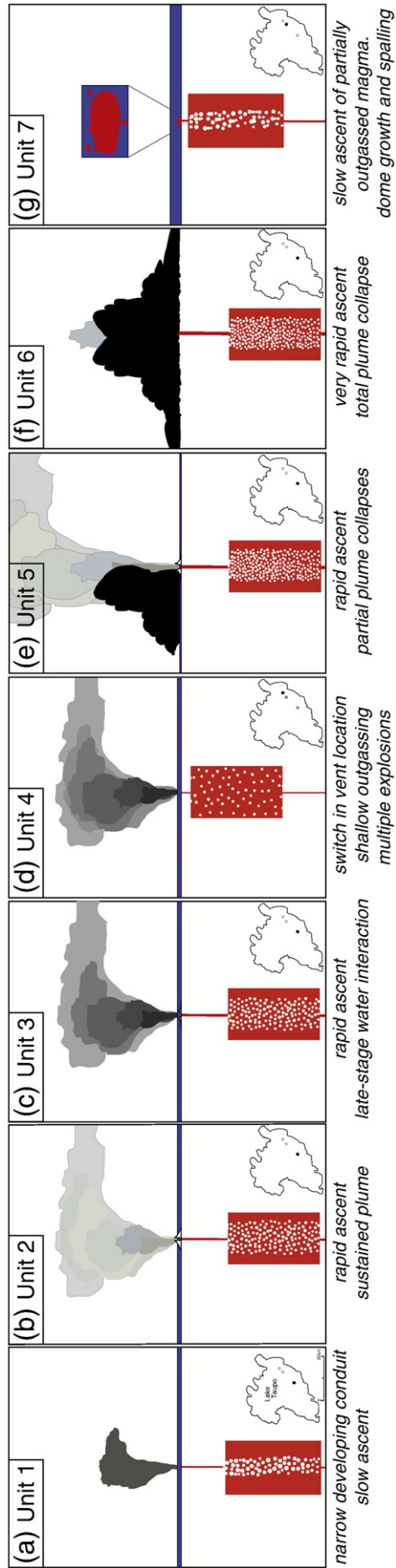


Fig. 13. Cartoon of changes in conduit, eruption and plume dynamics during the 1.8 ka Taupo eruption. Inset map shows the likely location of the vent(s) for each phase of the eruption.

consequence, permitting renewed egress of water to the vent and triggering a resumption of phreatomagmatic explosivity (unit 3).

Unit 3 is the product of this phreatomagmatism. The grain size of the unit 3 deposits suggest that initially there was a period of alternation between low and high magma/water ratios before a period of protracted phreatoplinian eruption interrupted by one brief reversion to relatively dry eruption (subunit 3c). Tephra dispersal suggests that the mass discharge rates represented by Plinian unit 2 were maintained during unit 3 times and the microtextures similarly imply a comparable history of conduit ascent and degassing. We favour, for this reason, very late and very shallow interaction with lake water which had a strong influence on deposit grain size and plume dynamics but negligible influence on eruption process (Fig. 13c).

Units 1, 2 and 3 are similar in lacking any evidence for shallow open-system behavior of the melt or outgassing at shallow level. Unit 4, erupted from a new vent location, contrasts markedly with its predecessors in many ways. The mm-bedded character of the deposits suggests the eruption was never sustained, even on timescales of minutes. Sharp changes in grain size favor abrupt shifts in both eruption intensity and magma:water ratio. A scarcity of true wall rock lithics suggests fragmentation was at shallow level and largely confined to the magma. Equally well, the Unit 4 pyroclasts show the most diverse range of microtextures in the Taupo eruption. These clasts have textures strongly suggestive of prolonged bubble development and establishment of permeable networks leading to variable amounts of outgassing. Smith and Houghton (1995) established that unit 4 was erupted from a source vent 10 km north of the unit 3 vent. We suggest that extension and widening of the eruptive fissure northeastward, at the close of unit 3 times, tapped into a shallow body of partially outgassed magma which was responsible for the Unit 4 eruption (Fig. 13d).

Field evidence suggests there was a brief overlap between unit 4 volcanism and the onset of eruption of unit 5 probably from another part of the vent system. This most powerful of Plinian eruptions was markedly less stable than that of unit 2, being characterized by fluctuations in mass discharge rate and punctuated by short-lived partial column collapses generating low-energy pyroclastic density currents (Fig. 13e). The next phase of our work will examine whether fluctuations in mass discharge and onset of short-lived plume collapses can be linked to microtextures in the erupted pyroclasts.

Instability and complete and permanent collapse of the plume then occurred during unit 6 times (Fig. 13f).

A significant time break, probably years to decades (Wilson and Walker 1985) is postulated between units 6 and 7. The Unit 7 blocks contain ample evidence for onset of permeability and partial degassing suggesting that this melt was resident beneath the central portion of the vent system for at least part of this time (Fig. 13g).

8. Conclusions

Intrusion along a 10 km dike permitted contrasting vesiculation histories in chemically extremely uniform magma which strongly governed mass discharge rates and modulated magma:water ratios. Judging by its limited crystallinity, the Taupo magma had undergone only very limited storage prior to its final ascent. The high N_v values for 'microvesicular' pumice reflects rapid nucleation and limits dominant bubble size (mostly 10–20 μm ; and <10 μm in some Plinian pumices). These high to very high vesicle number densities suggest moderately high to high rates of ascent through the conduit, which was then followed by divergence in patterns of late-stage vesiculation and ascent.

The highest vesicle number densities exist in pumices from the two highest intensity phases of the Taupo eruption, and reflect the most rapid ascent culminating in a late-stage supersaturation nucleation of bubbles under conditions of high volatile supersaturation. Application of the BND decompression rate meter of Toramaru (2006) to these clasts suggests decompression rates as high as $10^7 \text{ Pa}\cdot\text{s}^{-1}$. Fig. 12 suggests that there is a limiting value of N_v of $\sim 10^{10} \text{ cm}^{-3}$, which is perhaps linked to kinetics of

bubble formation. Maintaining this value also requires rapid quenching, as slower cooling typically allows bubble coalescence with a consequent decrease in N_v (e.g., the clasts from the unit 6 ignimbrite). These and other extremely vesicular clasts in the Taupo eruption reflect extensive bubble coalescence, with or without stretching. Such coalescence appears to have taken place under three separate sets of conditions:

- (1) Uniformly in the slower ascending magmas often followed by onset of permeability and partial outgassing (e.g., units 1, 4 and 7).
- (2) Post-fragmentation, in the cores of the larger pumices transported within the pyroclastic density currents of units 5B and 6.
- (3) In patchy fashion, to a limited extent, in the fall pumices (units 2, 3 and 5). The transformation from a microvesicular type A pumice with 75% vesicles to a type B pumice with 93% vesicles induces a 4.6 \times increase in bulk magma volume. We suggest therefore that the patchy onset of coalescence in the very shallow conduit may have driven the final non-linear acceleration of melt through the glass transition and fragmentation.

The least vesicular clasts did not fragment as they first attained a minimum vesicularity necessary for fragmentation, instead relatively mature textures with abundant coalesced bubbles, suggest that they fragmented late in their vesiculation history after the onset of permeability and bubble collapse.

The extent of textural diversity between clasts within a single samples and even within clasts suggest that at any single instant and during every explosive phase the fragmentation surface intersected melt in variable states of vesiculation and degassing. This diversity is greatest in samples that equate to the lowest eruption rates (e.g., unit 4), where there is clear textural evidence of partial outgassing, and the most uniform clast assemblages equate to the highest eruption rates (e.g., units 5a, 5b and 6).

Acknowledgements

This research was funded via a grant from the New Zealand Marsden Fund, NSF Grant EAR-0739060 and a subcontract from the New Zealand Foundation for Research, Science & Technology, via GNS Science. Image processing was performed by Jo Chizmar, Anne Duncan, Rosalind Houghton and Sarah Houghton. We acknowledge generous and constructive reviews by Steve Self and an anonymous reviewer.

References

- Adams, N.K., Houghton, B.F., Hildreth, W., 2006a. Abrupt transitions during sustained explosive eruptions: examples from the 1912 eruption of Novarupta, Alaska. *Bull. Volcanol.* 69, 189–206.
- Adams, N.K., Houghton, B.F., Fagents, S.A., Hildreth, W., 2006b. The transition from explosive to effusive eruptive regime: the example of the 1912 Novarupta eruption, Alaska. *Geol. Soc. Am. Bull.* 118, 620–634.
- Barberi, F., Cioni, R., Rosi, M., Santacroce, R., Sbrana, A., Vecchi, R., 1989. Magmatic and phreatomagmatic phases in explosive eruptions of Vesuvius as deduced by grain-size and component analysis of the pyroclastic deposits. *J. Volcanol. Geotherm. Res.* 38, 287–307.
- Blower, J.D., Keating, J.P., Mader, H.M., Phillips, J.C., 2002. The evolution of bubble size distributions in volcanic eruptions. *J. Volcanol. Geotherm. Res.* 120, 1–23.
- Blundy, J., Cashman, K., 2001. Magma ascent and crystallization at Mount St. Helens, 1980–1986. *Contrib. Mineral. Petrol.* 140, 631–650.
- Blundy, J., Cashman, K., 2005. Rapid decompression-driven crystallization recorded by melt inclusions from Mount St. Helens volcano. *Geology* 33, 793–796.
- Bower, S.M., Woods, A.W., 1998. On the influence of magma chambers in controlling the evolution of explosive volcanic eruptions. *J. Volcanol. Geotherm. Res.* 86, 67–78.
- Carey, R.J., Houghton, B.F., Sable, J.E., Wilson, C.J.N., 2007. Contrasting grain size and componentry in complex proximal deposits of the 1886 Tarawera basaltic Plinian eruption. *Bull. Volcanol.* 70, 903–926.
- Carey, R.J., Houghton, B.F., Thordarson, T., 2009. Abrupt shifts between wet and dry phases of the 1875 eruption of Askja Volcano: microscopic evidence for macroscopic dynamics. *J. Volcanol. Geotherm. Res.* 184, 256–270.
- Cashman, K.V., 1992. Groundmass crystallization of Mount St. Helens dacite, 1980–1986: a tool for interpreting shallow magmatic processes. *Contrib. Mineral. Petrol.* 109, 431–449.
- Cashman, K.V., Mangan, M.T., 1994. Physical aspects of magmatic degassing. 2. Constraints on vesiculation processes from textural studies of eruptive products. *Rev. Mineral.* 30, 447–478.
- Cioni, R., 2000. Volatile content and degassing processes in the AD 79 magma chamber at Vesuvius (Italy). *Contrib. Mineral. Petrol.* 140, 40–54.

- Cluzel, N., Laporte, D., Provost, A., Kannewischer, I., 2008. Kinetics of heterogeneous bubble nucleation in rhyolitic melts: implications for the number density of bubbles in volcanic conduits and for pumice textures. *Contrib. Mineral. Petrol.* 156, 745–763.
- Denlinger, R.P., Hoblitt, R.P., 1999. Cyclic eruptive behavior of silicic volcanoes. *Geology* 27, 459–462.
- Dunbar, N.W., Kyle, P.R., 1993. Lack of volatile gradient in the Taupo Plinian–ignimbrite transition: evidence from melt inclusion analysis. *Am. Mineral.* 78, 612–618.
- Fierstein, J., Hildreth, W., 1992. The Plinian eruptions of 1912 at Novarupta, Katmai National Park, Alaska. *Bull. Volcanol.* 54, 646–684.
- Fink, J.H., Anderson, S.W., Manley, C.R., 1992. Textural constraints on effusive silicic volcanism: beyond the permeable foam model. *J. Geophys. Res.* 97, 9073–9083.
- Gardner, J.E., 2007. Heterogeneous bubble nucleation in highly viscous silicate melts during instantaneous decompression from high pressure. *Chem. Geol.* 236, 1–12.
- Gardner, J.E., Thomas, R.M.E., Jaupart, C., Tait, S., 1996. Fragmentation of magma during Plinian volcanic eruptions. *Bull. Volcanol.* 58, 144–162.
- Gonnermann, H.M., Manga, M., 2007. The fluid mechanics inside a volcano. *Ann. Rev. Earth Planet. Sci.* 39, 321–356.
- Gurioli, L., Houghton, B.F., Cashman, K.V., Cioni, R., 2005. Complex changes in eruption dynamics during the 79 AD eruption of Vesuvius. *Bull. Volcanol.* 67, 144–159.
- Hammer, J.E., Manga, M., Cashman, K.V., 1998. Non-equilibrium and unsteady fluid degassing during slow decompression. *Geophys. Res. Lett.* 25, 4565–4568.
- Hammer, J.E., Cashman, K.V., Hoblitt, R.P., Newman, S., 1999. Degassing and microlite crystallization during pre-climactic events of the 1991 eruption of Mt. Pinatubo, Philippines. *Bull. Volcanol.* 60, 355–380.
- Hess, K.U., Dingwell, D.B., 1996. Viscosities of hydrous leucogranitic melts: a non-Arrhenian model. *Am. Mineral.* 81, 1297–1300.
- Hildreth, W., Fierstein, J., 2000. Katmai volcanic cluster and the great eruption of 1912. *Geol. Soc. Am. Bull.* 112, 1594–1620.
- Houghton, B.F., Wilson, C.J.N., 1989. A vesicularity index for pyroclastic deposits. *Bull. Volcanol.* 51, 451–462.
- Houghton, B.F., Hobden, B.J., Cashman, K.V., Wilson, C.J.N., Smith, R.T., 2003. Large-scale interaction of lake water and rhyolitic magma during the 1.8 ka Taupo eruption, New Zealand. In: White, J.D.L., Smellie, J.L., Clague, D.A. (Eds.), *Explosive Subaqueous Volcanism*, 140. Am. Geophys. Un. Geophys. Monog., pp. 97–109.
- Houghton, B.F., Wilson, C.J.N., Fierstein, J., Hildreth, W., 2004. Complex proximal deposition during the Plinian eruptions of 1912 at Novarupta, Alaska. *Bull. Volcanol.* 66, 95–133.
- Huppert, H.E., 2000. Geological fluid mechanics. In: Batchelor, G.K., Moffatt, H.K., Worster, M.G. (Eds.), *Perspectives in Fluid Dynamics: A Collective Introduction to Current Research*. Cambridge University Press, pp. 447–506.
- Jaupart, C., 1996. Physical models of volcanic eruptions. *Chem. Geol.* 128, 217–227.
- Jaupart, C., Allegre, C.J., 1991. Gas content, eruption rate and instabilities of eruption regime in silicic volcanoes. *Earth Planet. Sci. Lett.* 102, 413–429.
- Jaupart, C., Tait, S., 1990. Dynamics of eruptive phenomena. *Rev. Mineral.* 24, 213–238.
- Kaminski, E., Jaupart, C., 1997. Expansion and quenching of vesicular magma fragments in Plinian eruptions. *J. Geophys. Res.* 102, 12187–12203.
- Klug, C., Cashman, K.V., 1994. Vesiculation of May 18, 1980, Mount St. Helens magma. *Geology* 22, 468–472.
- Klug, C., Cashman, K.V., Bacon, C.R., 2002. Structure and physical characteristics of pumice from the climactic eruption of Mount Mazama (Crater Lake), Oregon. *Bull. Volcanol.* 64, 486–501.
- Koyaguchi, T., Woods, A.W., 1996. On the formation of eruption columns following explosive mixing of magma and surface water. *J. Geophys. Res.* 101, 5561–5574.
- Llewellyn, E.W., Manga, M., 2005. Bubble suspension rheology and implications for conduit flow. *J. Volcanol. Geotherm. Res.* 143, 205–217.
- Manga, M., Castro, J., Cashman, K.V., Loewenberg, M., 1998. Rheology of bubble-bearing magmas. *J. Volcanol. Geotherm. Res.* 87, 15–28.
- Mangan, M.T., Cashman, K.V., 1996. The structure of basaltic scoria and reticulite and inferences for vesiculation, foam formation, and fragmentation in lava fountains. *J. Volcanol. Geotherm. Res.* 73, 1–18.
- Mangan, M.T., Sisson, T.W., 2000. Delayed, disequilibrium degassing in rhyolite magma: decompression experiments and implications for explosive volcanism. *Earth Planet. Sci. Lett.* 183, 441–455.
- Mangan, M.T., Sisson, T.W., Hankins, W.B., 2004. Decompression experiments identify kinetic controls on explosive silicic eruptions. *Geophys. Res. Lett.* 31, L08605. doi:10.1029/2004GL019509.
- Marsh, B.D., 1988. Crystal size distribution (CSD) in rocks and the kinetics and dynamics of crystallization I. Theory. *Contrib. Mineral. Petrol.* 99, 277–291.
- Massol, H., Jaupart, C., 1999. The generation of gas overpressure in volcanic eruptions. *Earth Planet. Sci. Lett.* 166, 57–70.
- Massol, H., Koyaguchi, T., 2005. The effect of magma flow on nucleation of gas bubbles in a volcanic conduit. *J. Volcanol. Geotherm. Res.* 143, 69–88.
- Melnik, O., Sparks, R.S.J., 1999. Nonlinear dynamics of lava dome extrusion. *Nature* 402, 37–41.
- Melnik, O., Sparks, R.S.J., 2002. Modelling of conduit flow dynamics during explosive activity at Soufrière hills volcano Montserrat. *Geol. Soc. London. Mem.* pp. 307–317.
- Mourtada-Bonnefoi, C.C., Laporte, D., 1999. Experimental study of homogeneous bubble nucleation in rhyolitic magmas. *Geophys. Res. Lett.* 26, 3505–3508.
- Mourtada-Bonnefoi, C.C., Laporte, D., 2002. Homogeneous bubble nucleation in rhyolitic magmas: an experimental study of the effect of H₂O and CO₂. *J. Geophys. Res.* 107. doi:10.1029/2001JB000290.
- Mourtada-Bonnefoi, C.C., Mader, H.M., 2004. Experimental observations of the effect of crystals and pre-existing bubbles on the dynamics and fragmentation of vesiculating flows. *J. Volcanol. Geotherm. Res.* 129, 83–97.
- Nakada, S., Motomura, Y., 1999. Petrology of the 1991–1995 eruption at Unzen: effusion pulsation and groundmass crystallization. *J. Volcanol. Geotherm. Res.* 89, 173–196.
- Nakada, S., Shimizu, H., Ohta, K., 1999. Overview of the 1990–1995 eruption at Unzen Volcano. *J. Volcanol. Geotherm. Res.* 89, 1–22.
- Nairn, I.A., Self, S., Cole, J.W., Leonard, G.S., Scutter, C., 2001. Distribution, stratigraphy, and history of proximal deposits from the c. AD 1305 Kaharoa eruptive episode at Tarawera volcano, New Zealand. *N.Z. J. Geol. Geophys.* 44, 467–484.
- Orsi, G., Gallo, G., Heiken, G., Wohletz, K., Yu, E., Bonani, G., 1992. A comprehensive study of pumice formation and dispersal – the Cretaceous Tephra of Ischia (Italy). *J. Volcanol. Geotherm. Res.* 53, 329–354.
- Papale, P., 2001. Dynamics of magma flow in volcanic conduits with variable fragmentation efficiency and nonequilibrium pumice degassing. *J. Geophys. Res.* 106, 11043–11065.
- Papale, P., Neri, A., Macedonio, G., 1998. The role of magma composition and water content in explosive eruptions. 1. Conduit ascent dynamics. *J. Volcanol. Geotherm. Res.* 87, 75–93.
- Polacci, M., Papale, P., Rosi, M., 2001. Textural heterogeneities in pumices from the climactic eruption of Mount Pinatubo, 15 June 1991, and implications for magma ascent dynamics. *Bull. Volcanol.* 63, 83–97.
- Rust, A.C., Cashman, K.V., 2004. Permeability of vesicular silicic magma: inertial and hysteresis effects. *Earth Planet. Sci. Lett.* 228, 93–107.
- Sable, J.E., Houghton, B.F., Wilson, C.J.N., Carey, R.J., 2006. Complex proximal sedimentation from Plinian plumes: the example of Tarawera 1886. *Bull. Volcanol.* 69, 89–103.
- Sable, J.E., Houghton, B.F., Wilson, C.J.N., Carey, R.J., 2009. Eruption mechanisms during the climax of the Tarawera 1886 basaltic Plinian eruption inferred from microtextural characteristics of the deposits. In: Thorndarson, T., Self, S., Larsen, G., Rowland, S.K., Hoskuldsson, A. (Eds.), *Studies in Volcanology: The Legacy of George Walker*. IAVCEI Spec. Pub. 2. Geological Society, London, pp. 129–154.
- Sahagian, D.L., Proussevitch, A.A., 1998. 3D particle size distributions from 2D observations: stereology for natural applications. *J. Volcanol. Geotherm. Res.* 84, 173–196.
- Scandone, R., Cashman, K.V., Malone, S.D., 2007. Magma supply, magma ascent and the style of volcanic eruptions. *Earth Planet. Sci. Lett.* 253, 513–529.
- Shea, T., Larsen, J.F., Gurioli, L., Hammer, J.E., Houghton, B.F., Cioni, R., 2009. Leucite crystals: surviving witnesses of magmatic processes preceding the 79 AD eruption at Vesuvius, Italy. *Earth Planet. Sci. Lett.* 281, 88–98.
- Shea, T., Houghton, B.F., Gurioli, L., Cashman, K.V., Hammer, J.E., Hobden, B.J., 2010. Textural studies of vesicles in volcanic rocks: an integrated methodology. *J. Volcanol. Geotherm. Res.* 190, 271–289.
- Smith, R.T., 1998. Models for units 2 and 3 of the Taupo eruption. Ph.D. thesis, University of Canterbury, Christchurch, New Zealand.
- Smith, R.T., Houghton, B.F., 1995. Vent migration and changing eruptive style during the 1800a Taupo eruption: new evidence from the Hatepe and Rotongaio phreatoplinian ashes. *Bull. Volcanol.* 57, 432–439.
- Sparks, R.S.J., 1978. The dynamics of bubble formation and growth in magmas: a review and analysis. *J. Volcanol. Geotherm. Res.* 3, 1–37.
- Sparks, R.S.J., Brazier, S., 1982. New evidence for degassing processes during explosive eruptions. *Nature* 295, 218–220.
- Sutton, A.N., Blake, S., Wilson, C.J.N., 1995. An outline geochemistry of rhyolite eruptives from Taupo volcanic centre, New Zealand. *J. Volcanol. Geotherm. Res.* 68, 153–175.
- Sutton, A.N., Blake, S., Wilson, C.J.N., Charlier, B.L.A., 2000. Late Quaternary evolution of a hyperactive rhyolite magmatic system: Taupo volcanic centre, New Zealand. *J. Geol. Soc. Lond.* 157, 537–552.
- Toramaru, A., 1990. Measurement of bubble-size distributions in vesiculated rocks with implications for quantitative estimation of eruption processes. *J. Volcanol. Geotherm. Res.* 43, 71–90.
- Toramaru, A., 1995. Numerical study of nucleation and growth of bubbles in viscous magmas. *J. Geophys. Res.* 100, 1913–1931.
- Toramaru, A., 2006. BND (bubble number density) decompression rate meter for explosive volcanic eruptions. *J. Volcanol. Geotherm. Res.* 154, 303–316.
- Walker, G.P.L., 1980. The Taupo Pumice: product of the most powerful known (ultraplinian) eruption? *J. Volcanol. Geotherm. Res.* 8, 69–94.
- Walker, G.P.L., 1981a. The Waimihia and Hatepe Plinian deposits from the rhyolitic Taupo volcanic centre. *N.Z. J. Geol. Geophys.* 24, 305–324.
- Walker, G.P.L., 1981b. Characteristics of two phreatoplinian ashes and their water-flushed origin. *J. Volcanol. Geotherm. Res.* 9, 395–407.
- Whitham, A.G., Sparks, R.S.J., 1986. Pumice. *Bull. Volcanol.* 48, 209–223.
- Wilson, C.J.N., 1985. The Taupo eruption, New Zealand II. The Taupo ignimbrite. *Phil. Trans. Roy. Soc. Lond.* A314, 229–310.
- Wilson, C.J.N., 1993. Stratigraphy, chronology, styles and dynamics of late Quaternary eruptions from Taupo volcano, New Zealand. *Phil. Trans. Roy. Soc. Lond.* A343, 205–306.
- Wilson, C.J.N., Walker, G.P.L., 1981. Violence in pyroclastic flow eruptions. In: Self, S., Sparks, R.S.J. (Eds.), *Tephra Studies*. D. Reidel, Dordrecht, Netherlands, pp. 441–448.
- Wilson, C.J.N., Walker, G.P.L., 1985. The Taupo eruption, New Zealand I. General aspects. *Phil. Trans. Roy. Soc. Lond.* A314, 199–228.
- Wilson, L., Sparks, R.S.J., Walker, G.P.L., 1980. Explosive volcanic eruptions – IV. The control of magma properties and conduit geometry on eruption column behaviour. *Geophys. J. R. Astron. Soc.* 63, 117–148.
- Woods, A.W., Koyaguchi, T., 1994. Transitions between explosive and effusive eruptions of silicic magmas. *Nature* 370, 641–644.
- Wright, H.M.N., Weinberg, R.F., 2009. Strain localization in vesicular magma: implications for rheology and fragmentation. *Geology* 37, 1023–1026.
- Wright, H.M.N., Roberts, J.J., Cashman, K.V., 2006. Permeability of anisotropic tube pumice: model calculations and measurements. *Geophys. Res. Lett.* 33 (17) Article L17316.